

*Reprints of
Published Papers*

New empirical formula for (γ, n) reaction cross section near GDR Peak for elements with $Z \geq 60$ *

Rajnikant Makwana^{1,1)} S. Mukherjee¹ Jian-Song Wang(王建松)² Zhi-Qiang Chen(陈志强)²

¹ Physics Department, Faculty of Science, The Maharaja Sayajirao University of Baroda, Vadodara-390002, India

² Key Laboratory of High Precision Nuclear Spectroscopy and Center for Nuclear Matter Science, Institute of Modern Physics, Chinese Academy of Science, Lanzhou 730000, China

Abstract: A new empirical formula has been developed that describes the (γ, n) nuclear reaction cross sections for isotopes with $Z \geq 60$. The results were supported by calculations using TALYS – 1.6 and EMPIRE – 3.2.2 nuclear modular codes. The energy region for incident photon energy has been selected near the giant dipole resonance (GDR) peak energy. The evaluated empirical data were compared with available data in the experimental data library EXFOR. The data produced using TALYS – 1.6 and EMPIRE – 3.2.2 are in good agreement with experimental data. We have tested and presented the reproducibility of the present new empirical formula. We observe the reproducibility of the new empirical formula near the GDR peak energy is in good agreement with the experimental data and shows a remarkable dependency on key nuclei properties: the neutron, proton and atomic number of the nuclei. The behavior of nuclei near the GDR peak energy and the dependency of the GDR peak on the isotopic nature are predicted. An effort has been made to explain the deformation of the GDR peak in (γ, n) nuclear reaction cross sections for some isotopes, which could not be reproduced with TALYS – 1.6 and EMPIRE – 3.2.2. The evaluated data have been presented for the isotopes ^{180}W , ^{183}W , ^{202}Pb , ^{203}Pb , ^{204}Pb , ^{205}Pb , ^{231}Pa , ^{232}U , ^{237}U and ^{239}Pu , for which there are no previous measurements.

Keywords: photonuclear reactions, GDR, empirical formula, TALYS, EMPIRE, cross section

PACS: 25.20.-x **DOI:** 10.1088/1674-1137/41/4/044105

1 Introduction

Nuclear reactions are of prime importance in the application of nuclear reactor technology. Nuclear reactors (fusion-fission) require a complete dataset of neutron and photon induced reactions. Photonuclear reactions are becoming more important for fusion reactors and accelerator driven sub-critical system (ADS), where high-energy photons will be generated and subsequently interact with the materials. The study of (γ, n) reactions are important for a variety of current and emerging fields, such as radiation shielding design, radiation transport, absorbed dose calculations for medical, physics, technology of fusion-fission reactors, nuclear transmutation, and waste management applications [1,2]. In a fusion reactor, during the plasma shot, de-confined runaway electrons can interact with the first wall of the reactor and produce high energy photons [3]. These high energy photons can open reaction channels like (γ, n) , (γ, p) , $(\gamma, 2n)$, $(\gamma, 3n)$, etc. The most prominent reaction is (γ, n) , as it has a lower threshold than multi-

neutron emission, whereas for charged particle emission the Coulomb barrier needs to be considered. Exact information on the cross section for such nuclear reactions is needed to perform accurate nuclear transport calculations. Tungsten (W) and beryllium (Be) are selected as first wall materials for the International Thermonuclear Experimental Reactor (ITER) fusion reactor [4]. Among tungsten isotopes, only ^{182}W (26.5 %), ^{184}W (30.64%) and ^{186}W (28.43%) have experimental cross section data for the (γ, n) reaction. The cross sections of the (γ, n) reaction for ^{180}W (0.12%) and ^{183}W (14.31%) are needed, along with all the remaining long-lived unstable isotopes, as they will interact with high-energy photons during the confined runaways and disruption phase [5]. Gamma induced nuclear reactions are also important for nuclear transmutation (e.g. $^{234}\text{U}(\gamma, n)^{233}\text{U}$), which is useful for nuclear safety and incineration. The importance of the gamma incineration technique has been studied in the case of many isotopes for nuclear waste management [6–8].

In ADSs, the high energy proton beam will inter-

Received 30 May 2016

*

1) E-mail: rajniipr@gmail.com

©2017 Chinese Physical Society and the Institute of High Energy Physics of the Chinese Academy of Sciences and the Institute of Modern Physics of the Chinese Academy of Sciences and IOP Publishing Ltd

act with high Z elements such as W, Pb-Bi, Th and U, which will produce neutrons through spallation reactions [9]. This spallation process will produce high energy photons, which will subsequently interact with the materials. It is necessary to have a complete nuclear dataset of photonuclear reactions for all isotopes of these elements. This can be done by experimental measurements. The experimental measurements of the nuclear reaction cross-section are one of the important methods to complete the nuclear dataset. However, there are always limitations in the experimental measurements due to non-availability of all the energies of incident particles, and preparation of the target, which may itself be unstable. For complete nuclear data for several isotopes, nuclear modular codes such as TALYS – 1.6 and EMPIRE – 3.2.2 are available. Using these codes, one can predict the cross sections for different nuclear reaction channels. These codes basically use some nuclear models, and on the bases of the nuclear reaction theory, evaluation of the nuclear reaction data is done. The theory involved in photonuclear reaction cross section evaluation is discussed in the next section of the paper. Apart from this, nuclear systematics and empirical formulae provide alternative methods for such isotopes, and can efficiently predict the nuclear properties. Many authors have used this theoretical approach. Several systematics and empirical studies have already been made for photonuclear reactions [10]. These empirical formulae reduce experimental efforts, as they are basically dependent on well-known nuclear properties. A new empirical formula has been developed and tested with nuclear modular codes and experimental data for $Z \geq 60$ in the present paper. With the help of the present empirical formula, one can predict the cross section datasets for those isotopes where there is a complete lack of experimental data.

2 Theory of photo neutron production

The interaction of high energy photons with target material can cause ejection of the nucleon/s, depending upon the energy of the incident photon. This reaction is considered a photonuclear reaction. Photons should have sufficient energy above the binding energy of the nucleus for nucleon emission. As the nuclear binding energies are above 6 MeV for most isotopes, photons should have such a threshold energy [11]. There are three basic mechanisms for photonuclear reactions: (a) giant dipole resonance (GDR), (b) quasi-deuteron (QD) and (c) intra-nuclear cascade [12]. A photon with energy below 30 MeV follows the GDR mechanism. In this process, the photon energy is transferred to the nucleus by the oscillating electrical field of the photon, which induces oscillations among nucleons inside the nucleus. Photo neutron production is more probable since proton ejection

needs to overcome a large Coulomb barrier. For different isotopes at a particular energy, there is a peak of photo neutron production for the (γ, n) reaction. This is called the GDR peak energy. For isotopes above $Z = 60$, the peak energies are between 10-18 MeV. Above 30 MeV, the photo neutron production is mainly due to the QD effect [12]. In this mechanism, a photon interacts with the dipole moment of a pair of proton-neutrons in place of the nucleus as a whole [12]. Above 140 MeV, photo neutron production results from photo-pion production [12]. Further study of thermal fluctuation on GDR parameters is also of interest and studies are ongoing [13–16].

3 Present empirical formula and theoretical calculations

According to the semi-classical theory of the interaction of photons with nuclei, the shape of the fundamental resonance of the photo absorption cross section follows a Lorentz curve [12, 17].

$$\sigma(E) = \frac{\sigma_i}{1 + \left[\frac{(E_\gamma^2 - E_m^2)^2}{E_\gamma^2 \gamma^2} \right]}, \quad (1)$$

where, σ_i , E_γ and γ are the Lorentz parameters: peak cross section, resonance energy and full width at half maximum respectively [18].

In a more general way, by using nuclear modular codes, such as TALYS – 1.6 and EMPIRE – 3.2.2, the photo absorption cross section is calculated as the sum of two components [19],

$$\sigma_{\text{abs}}(E_\gamma) = \sigma_{\text{GDR}}(E_\gamma) + \sigma_{\text{QD}}(E_\gamma). \quad (2)$$

The component $\sigma_{\text{GDR}}(E_\gamma)$ represents the GDR and is given by a Lorentzian shape, which describes the giant dipole resonance. It is given from Eq. (1) by the following expression:

$$\sigma(E) = \sum_i \frac{\sigma_i \cdot (E_\gamma \cdot \Gamma_i)^2}{(E_\gamma^2 - E_i^2)^2 + (E_\gamma \cdot \Gamma_i)^2}, \quad (3)$$

where σ_i , E_i and Γ_i are: peak cross section, resonance energy and full width at half maximum respectively. The summation is limited to $i = 1$ for spherical nuclei, while for deformed nuclei the resonance is split and one uses $i = 1, 2$. The component $\sigma_{\text{QD}}(E_\gamma)$, is given by Levinger type theory given by Chadwick et al [19–21]. It is basically from the quasi-deuteron model. In the energy range from the photonuclear threshold to 30 MeV, the GDR mechanism is dominant, and from 30 – 140 MeV the QD mechanism is dominant. Above 140 MeV the threshold energy for pion production is achieved [20].

The above theory has been used in the TALYS – 1.6 and EMPIRE – 3.2.2 nuclear modular codes [22, 23].

Further details of these codes are given in Refs. [18, 24]. Using these codes, (γ, n) nuclear reaction cross sections for different isotopes ($Z \geq 60$) were calculated and are presented in the present work. Until now, the photonuclear reaction cross sections have been evaluated using the Lorentz parameters. These parameters for several isotopes are calculated by fitting the experimental data or by systematics [25].

3.1 Fundamental term

In the present paper, in contrast to the Lorentzian parameters, the basic properties of nuclei, A , N and Z , are used to estimate the photonuclear cross section. Levovskii has given empirical formulas for (n, p) and $(n, 2n)$ reaction cross section at 14.0 MeV [26] as,

$$\sigma(n, p) \propto \sigma_p \cdot e^{-\frac{33 \cdot (N-Z)}{A}}, \quad (4)$$

$$\sigma(n, 2n) \propto \sigma_\alpha \cdot e^{-\frac{33 \cdot (N-Z)}{A}}, \quad (5)$$

where $\sigma_p = \pi r_0^2 (A^{1/3} + 1)^2$ and $\sigma_\alpha = 0.4 \cdot \pi r_0^2 (A^{1/3} + 1)^2$, $r_0 = 1.2 \times 10^{-13}$ cm.

These empirical formulae are based on A , N and Z of a nucleus, and at an energy 14.0 MeV. Similarly it is possible to derive an empirical formula for photo induced (γ, n) nuclear reactions, which may be applied near GDR peak energy. For the (γ, n) reaction, the formula is modified in the following way,

$$\sigma(\gamma, n) \propto \sigma_m \cdot e^{-\frac{33.5 \cdot (N-Z)}{A}}, \quad (6)$$

$$\sigma_m = \pi r_0^2 \cdot (A^{2/3} + 1)^2 \cdot (N-Z) \cdot A^{-\frac{4}{3}}, \quad (7)$$

where r_0 is the average nuclear radius.

3.2 Isotopic dependent resonance term

The term $(N-Z)/A$ is the asymmetry parameter which considers the deformation of a nucleus. In this expression, there is no term containing energy dependency. Hence, an energy dependent term must be added, and the modified formula is as given below,

$$\sigma(\gamma, n) \propto \sigma_m \cdot e^{-\frac{33.5 \cdot (N-Z)}{A}} \cdot e^{-\left(\frac{E_i - S_j \cdot R_p}{2}\right)^2} \quad (8)$$

where E_i is the incident photon energy, and R_p is the resonance parameter.

The parameter S_j is given by,

$$S_j = \frac{A^2}{2(N-Z)^2}. \quad (9)$$

The parameter R_p is estimated for an isotope by fitting the (γ, n) nuclear reaction cross section using the above formula for different isotopes of the same element. We

observed that this parameter R_p follows a linear relationship against the atomic mass of different isotopes of the same element, which can be written in the form of the following equation,

$$R_p = m \cdot A + C, \quad (10)$$

where A is the atomic mass of the isotope, and m and C are slope and intercept respectively. More details of this parameter (R_p) for different elements is given in Section 3.3.1.

This term $e^{-\left\{\frac{(E_i - S_j \cdot R_p)}{2}\right\}^2}$ depends on the energy of the incident photon and the isotopic nature of the target nucleus. When a photon is incident on the nucleus the response of the nucleus depends on the photon energy. While the incident photon is below the threshold energy for photo fission the photon cannot eject a nucleon from the nucleus. If energy of the photon is above the threshold energy of the (γ, n) reaction, the reaction cross section increases until the resonance peak energy. After this energy the cross section decreases again. This is incorporated using this exponential term. The subtraction of $S_j \cdot R_p$ from the incident photon energy shows the isotopic dependence of the resonance peak energy of the reaction. As the isotopic number increases it is observed in the experimental data that the GDR peak shifts towards the lower energy side. This back shift effect can be calculated with the exponential term considered here. The value of $S_j \cdot R_p$ increases with addition of neutrons to the isotope nucleus. This means that when a photon is incident on the target isotope, it interacts with the last shell neutron in the nucleus. The binding energy of the last added neutron will be least. Hence the photon may require smaller energy to cause the resonance as the isotope number increases

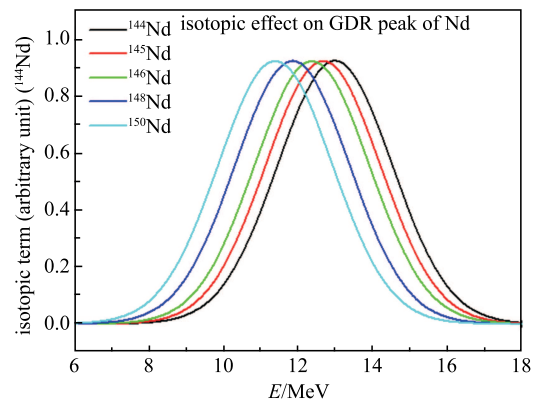


Fig. 1. (color online) Back shift of resonance peak energy in Nd isotopes, from the term $e^{-\left\{\frac{(E_i - S_j \cdot R_p)}{2}\right\}^2}$.

This can be observed from Figs. 1 and 2, showing the isotopic effect for the resonance peak energy back shift in Nd and Pt isotopes from the above exponential term.

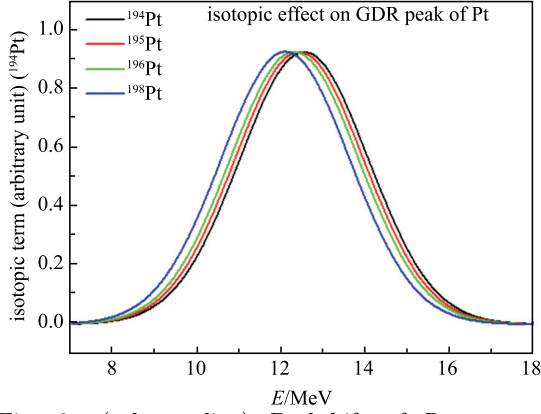


Fig. 2. (color online) Backshift of Resonance Peak Energy in Pt isotopes, from the term $e^{-\left\{\frac{(E_i - S_j \cdot R_p)}{2}\right\}^2}$.

3.3 Energy dependency term

It was found that another energy related term is required to make the formula more efficient to predict the cross section. If the photon energy increases, then the photon can transfer more energy to the nucleus. In the GDR mechanism, the oscillating electrical field transfers its energy to the nucleus by inducing an oscillation in the nucleus, which leads to relative displacement of tightly bound neutrons and protons inside the nucleus. [12]

When the energy of the photon is low (near threshold), the oscillating electric field of the photon interacts with the collective nucleus field produced by the sum effect of the nucleons. But as the energy of the photon increases, the oscillating electrical field interacts with a pair of neutron and proton rather than with the nucleus. This is followed by the term $e^{\sqrt{1+E^{\frac{2}{3}}}}$, where E is the energy of the incident photon. This term shows that the photon can have more energy to transfer to the nucleon as the incident photon energy increases. This indicates that as the energy of the photon increases, it can have less interaction time with nucleons, and hence the pre-equilibrium or direct reaction mechanism can be followed by the emission of the neutron.

Hence, by the addition of an energy dependent term, the modified formula is,

$$\sigma(\gamma, n) \propto \sigma_m \cdot e^{-\frac{33.5 \cdot (N-Z)}{A}} \cdot e^{-\left\{\frac{(E_i - S_j \cdot R_p)}{2}\right\}^2} \cdot e^{\sqrt{1+E^{\frac{2}{3}}}}. \quad (11)$$

An additional factor S_f , which is an isospin dependent factor, has been introduced to complete the formula. This factor was plotted for different isotopes of the same element, and fitted. We observed this factor follows some exponential relation, which is described in Section 3.3.2. This empirical formula gives the cross section to the order of milli-barns.

The final modified formula is now,

$$\sigma(\gamma, n) = \sigma_m \cdot e^{-\frac{33.5 \cdot (N-Z)}{A}} \cdot e^{-\left\{\frac{(E_i - S_j \cdot R_p)}{2}\right\}^2} \cdot e^{\sqrt{1+E^{\frac{2}{3}}}} \cdot S_f. \quad (12)$$

3.3.1 R_p parameter

This parameter shows the dependency of the photo absorption cross section with respect to the atomic number (Z). In the empirical formula, the term $e^{-\left\{\frac{(E_i - S_j \cdot R_p)}{2}\right\}^2}$ has a subtraction factor containing S_j and R_p . R_p is responsible for the change in the cross section due to atomic number, and the multiplication of S_j and R_p is responsible for the isotopic back shift effect, as shown in Figs. 1 and 2. The parameter R_p for different isotopes can be calculated using a linear relation, viz Eq. (10), with the atomic mass number of isotopes for an element. Therefore, the plot of R_p vs A for different elements should show parallel lines with different intercepts on the R_p axis, as shown in Fig. 3. Parallel lines have the same slope but different intercepts. Hence, the mean slope of different elements has been taken as the standard slope for all elements ($Z \geq 60$). This value of the slope (m) mentioned in Eq. (10) is $\sim 0.03164 \pm 0.00409$. The intercept C for different elements are plotted against the atomic number of the element, and fitted with the mathematical software MATLAB using a 3rd degree polynomial as shown in Fig. 4. The intercept C for different elements can be determined from the following equation:

$$C(Z) = p_1 \cdot Z^3 + p_2 \cdot Z^2 + p_3 \cdot Z + p_4 \quad (13)$$

with $p_1 = -4.155 \times 10^{-5}$, $p_2 = 0.008971$, $p_3 = -0.7156$, and $p_4 = 15.78$, where Z is atomic number (SSE: 0.00147; R-square: 0.9998; Adjusted R-square: 0.9996; RMSE: 0.01917).

Hence, the intercept for any element can be evaluated using the above Eq. (13). Using this intercept and the slope 0.03164 ± 0.00409 , one can calculate the parameter R_p from Eq. (10). The model values of the parameter R_p for different elements are compared with the previous manually selected values in Fig. 3.

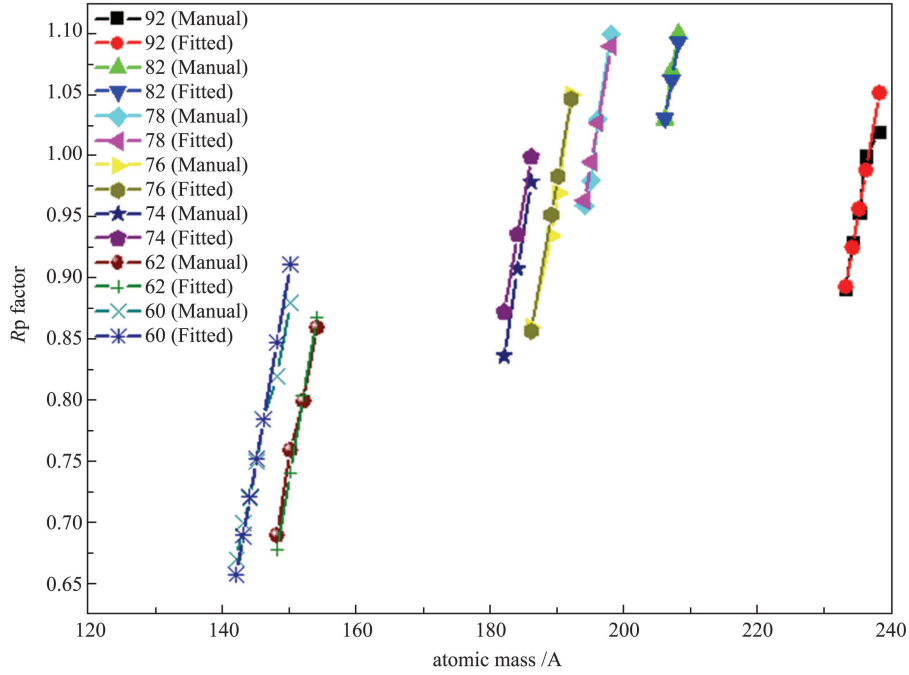


Fig. 3. (color online) R_p parameter fitting for different elements with Eq. (10).

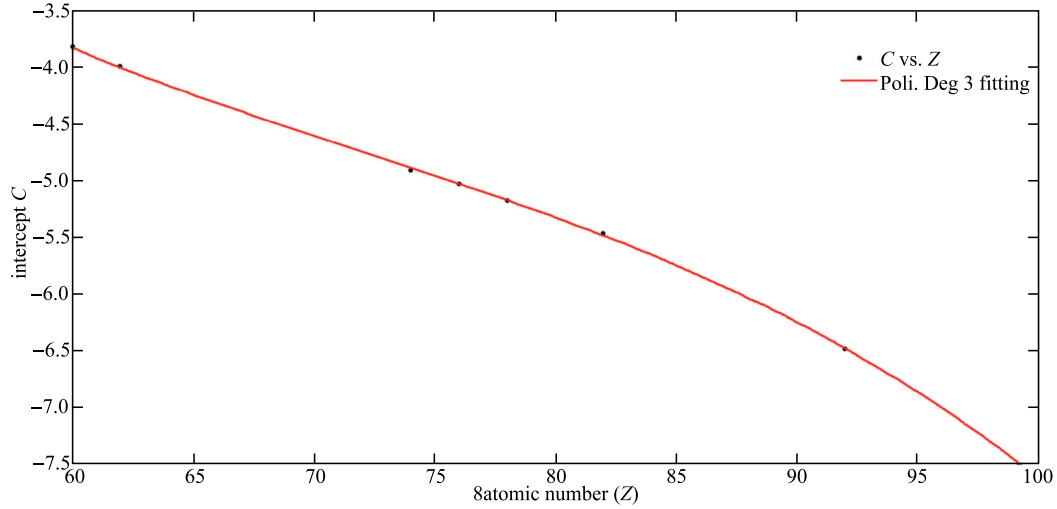


Fig. 4. Intercept C for Eq. (10) for different elements fitted with Eq. (11).

3.3.2 S_f Parameter

This parameter includes the isospin effect. This effect has been discussed by J. S. Wang et al. [27]. In order to include this effect in the empirical formula, an additional factor called S_f has been added. This factor was initially manually added and then, in order to generalize, it was fitted with different combinations of N , Z and A . It was found that it follows a complex exponential relation with $\exp((N-Z)/N)$ of an isotope. This parameter S_f is also considered a result of the asymmetry of the nucleus.

As there is a difference in neutron and proton number, the fraction $(N-Z)/N$ is the available neutron fraction for a photon to eject. As this fraction value increases, the value of S_f increases correspondingly, which directly shows an increase in the photo absorption cross section of that isotope.

This isotopic factor S_f for different isotopes is plotted with respect to $e^{\frac{N-Z}{N}}$ and fitted with MATLAB software as shown in Fig. 4. The generalized expression to determine the S_f parameter for an isotope is as given below:

$$S_f = ae^{bx} + ce^{dx}, \quad (14)$$

where, $x = (N - Z)/N$, $a = 1.21 \times 10^{-22}$, $b = 34.21$, $c = 7.71 \times 10^{-11}$, $d = 14.52$

(SSE: 0.006977; R-square: 0.9781; Adjusted R-square: 0.9759; RMSE: 0.01551).

Looking at Fig. 5 carefully, for some points when

$e^{\frac{(N-Z)}{N}}$ is near 1.40 to 1.42, they have almost the same S_f factor values. These S_f factor values are for $Z = 82$ and $N = 124, 125, 126$, which are either a magic number or near the magic number. S_f is purely dependent on $(N - Z)/N$, which is a shell dependent term. The anomalous behavior of the same S_f factor values for these isotopes is because of the magic shell effect.

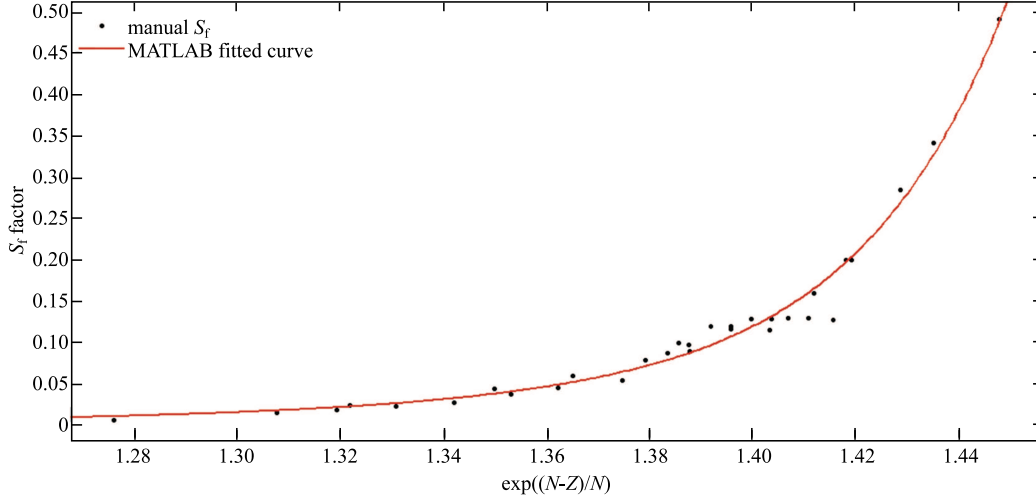


Fig. 5. S_f parameter for different $(N - Z)/N$ fitted with Eq. (14).

4 Results and discussion

The (γ, n) reaction cross sections are calculated using TALYS - 1.6, EMPIRE - 3.2.2 and the newly developed empirical formula for isotopes with $Z \geq 60$ and presented in Figs. 6–10. The cross sections are calculated for the energy range in which the GDR peak is observed. The theoretically calculated cross sections are compared with the experimentally available data in the EXFOR data library [28]. The data calculated using modular codes and empirical formula are in agreement with the experimental data, as shown in Figs. 6–10. However, the cross section values and the nuclear behavior near the GDR peak predicted by the empirical formula are more appropriate. This empirical formula is good for those isotopes which have a single GDR peak. In most of the cases studied here that have a single GDR peak, the empirical formula gives good agreement near the GDR peak energy compared to the model based on Lorentz curve fitting.

In the case of isotopes with Z from 63 to 75, it is found that according to the collective model these isotopes have large nuclear quadrupole moments. The quadrupole exists because of the asymmetry of the nucleus. The nuclei are found in the middle of the 1d, 2 s shells in the range $145 < A < 185$. The energy dif-

ference between the ground state and the first excited state is of the order of hundreds of keV. In the deformed nucleus the incident photon can interact either with the ground state or with the excited state nucleon, and hence can produce a resonance at two different nearby energies. This is observed in the above isotopes. For such cases, the Lorentz curve based model, viz. TALYS - 1.6 and EMPIRE - 3.2.2, works reliably for these isotopes, as shown in Fig. 11. For some cases, however, the TALYS - 1.6 and EMPIRE - 3.2.2 model does not work well, e.g. Figs. 11(e - f). To apply the empirical formula for such isotopes, it is assumed that there may be two peaks due to unresolved resonances occurring near the energies of ground and excited nuclei, which are due to the quadrupole moment. This suggests parameters R_p and S_f can have two different values for these isotopes. It indicates that the energy dependence cross section curve is made of two curves with two different R_p (R_{p1} and R_{p2}) and S_f values (S_{f1} and S_{f2}) of parameters R_p and S_f respectively. These values can be estimated by multiplying the following factors to the R_p and S_f values calculated from Sections 3.3.1 and 3.3.2.

$$R_{p1} = 0.95 \times R_p, \quad (15)$$

$$R_{p2} = 1.20 \times R_p, \quad (16)$$

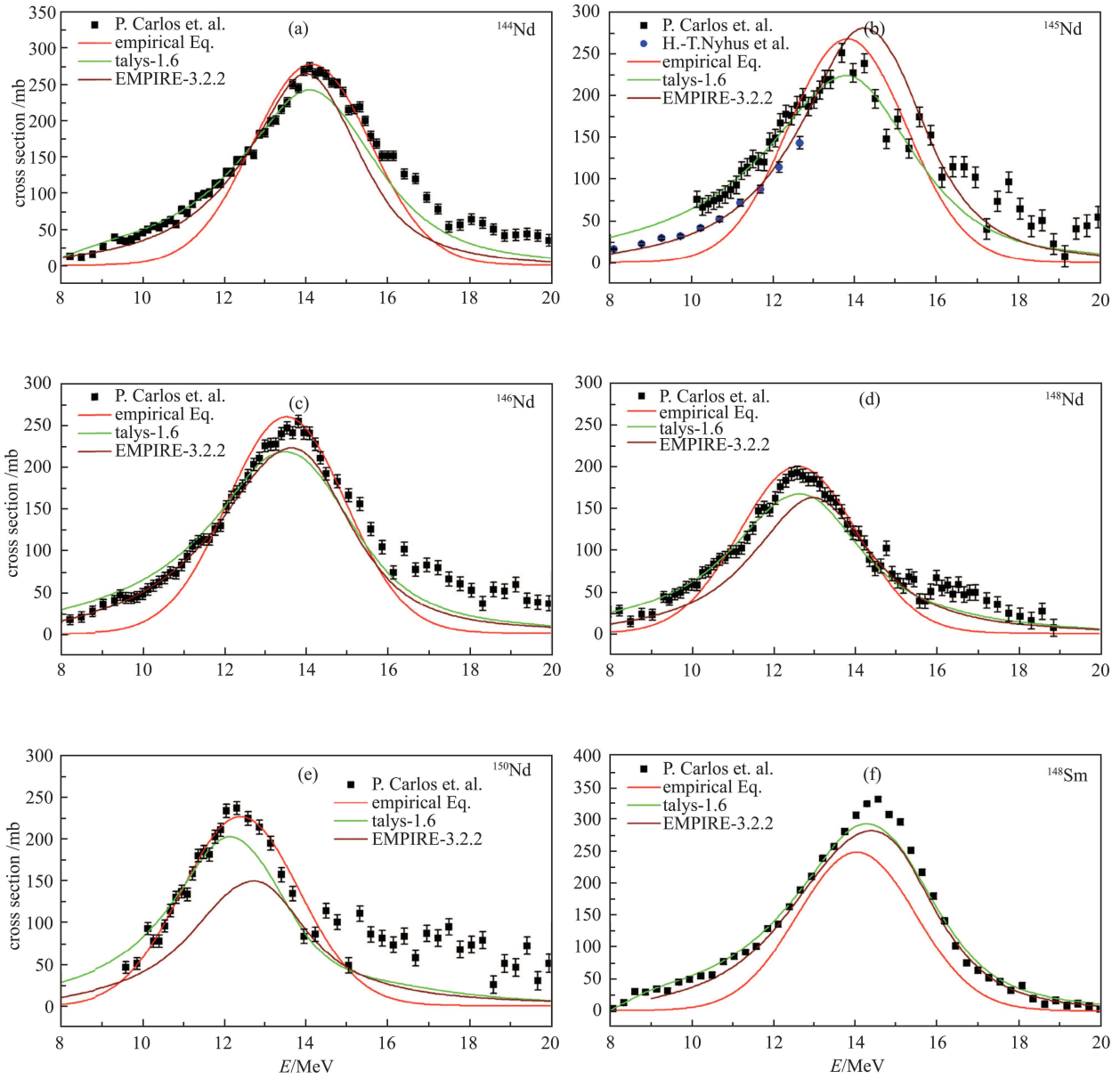


Fig. 6. (color online) Comparison of evaluated data using TALYS-1.6, EMPIRE-3.2.2, and empirical formula with experimental data from EXFOR, for ^{144}Nd , ^{145}Nd , ^{146}Nd , ^{148}Nd , ^{150}Nd , and ^{148}Sm .

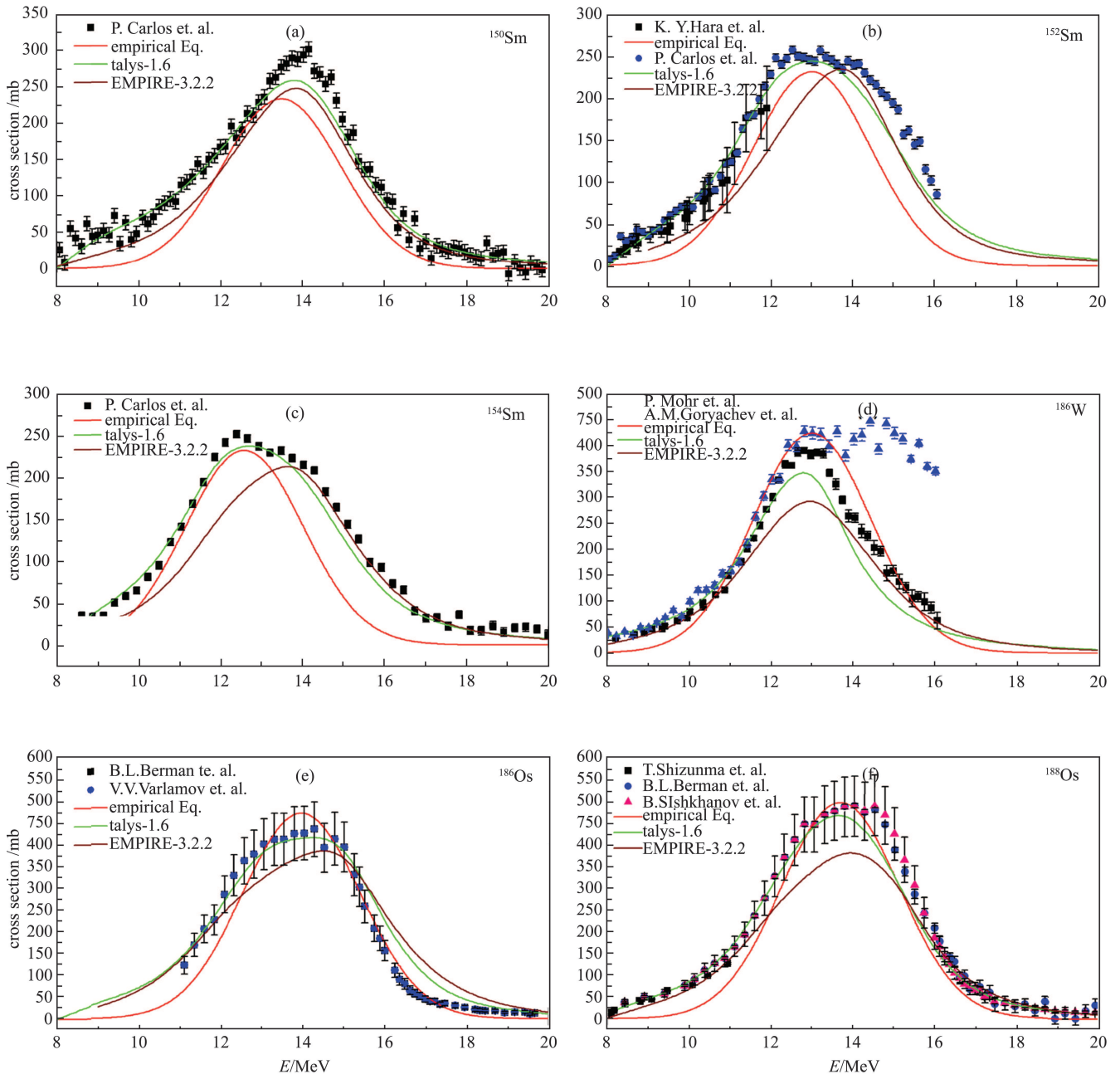


Fig. 7. (color online) Comparison of evaluated data using TALYS-1.6, EMPIRE-3.2.2, and empirical formula with experimental data from EXFOR, for ^{150}Sm , ^{152}Sm , ^{154}Sm , ^{186}W , ^{186}Os , and ^{188}Os .

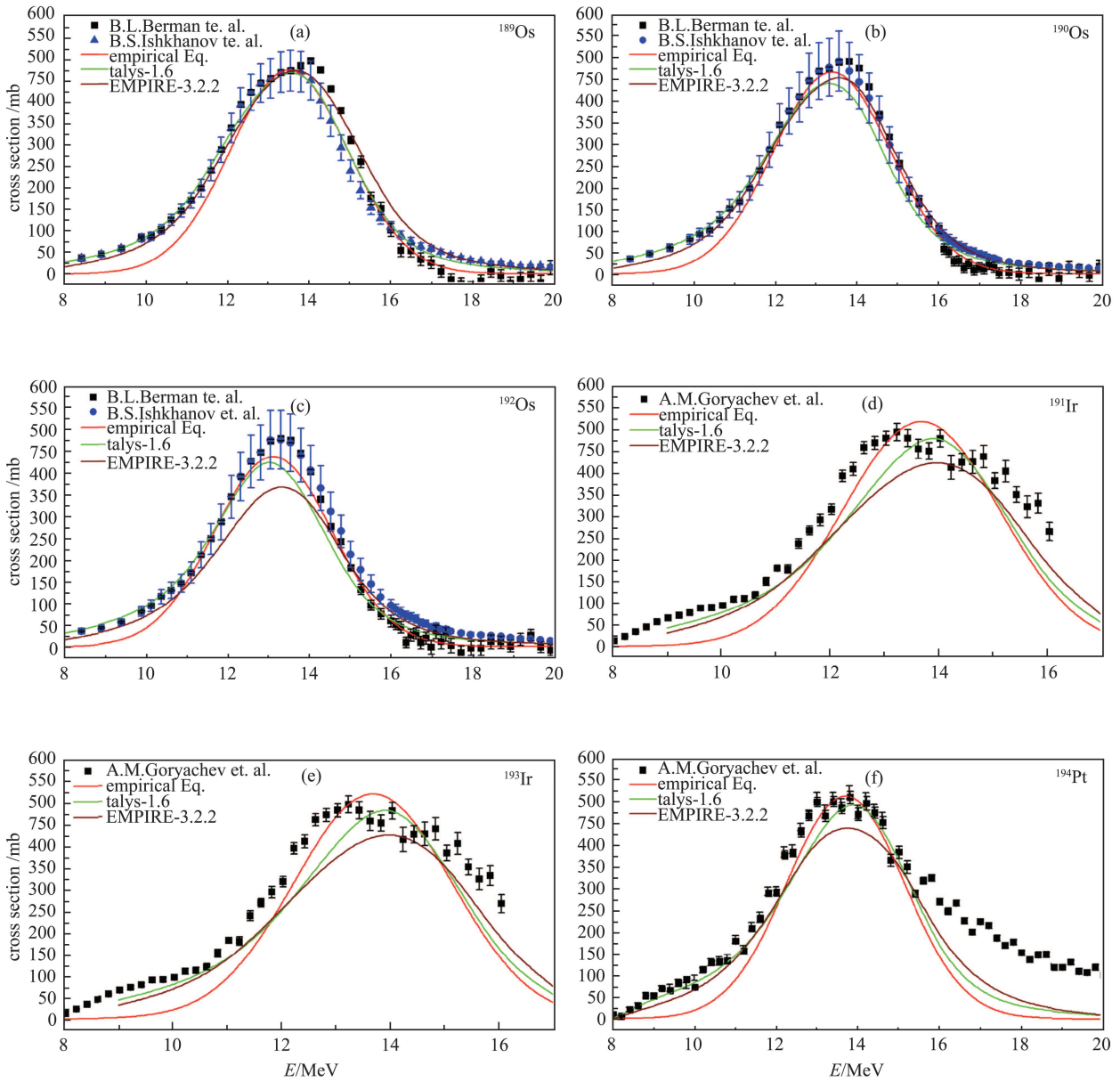
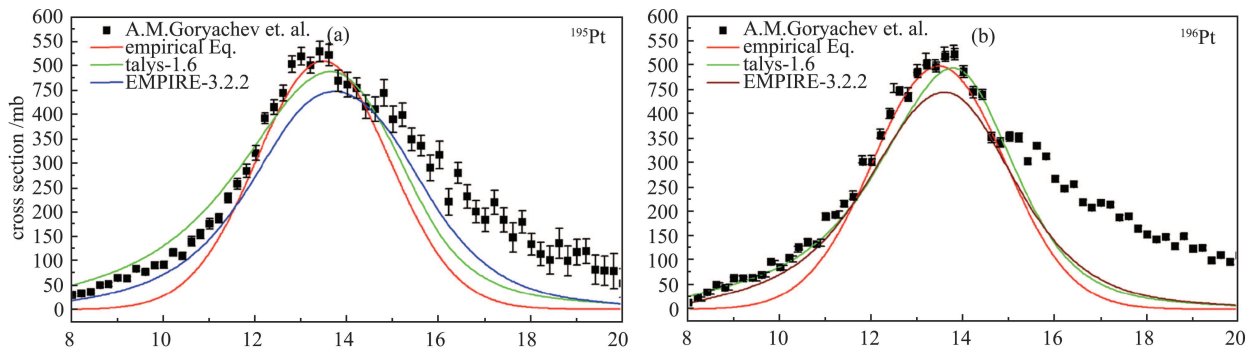


Fig. 8. (color online) Comparison of evaluated data using TALYS-1.6, EMPIRE-3.2.2, and empirical formula with experimental data from EXFOR, for ^{189}Os , ^{190}Os , ^{192}Os , ^{191}Ir , ^{193}Ir , and ^{194}Pt .



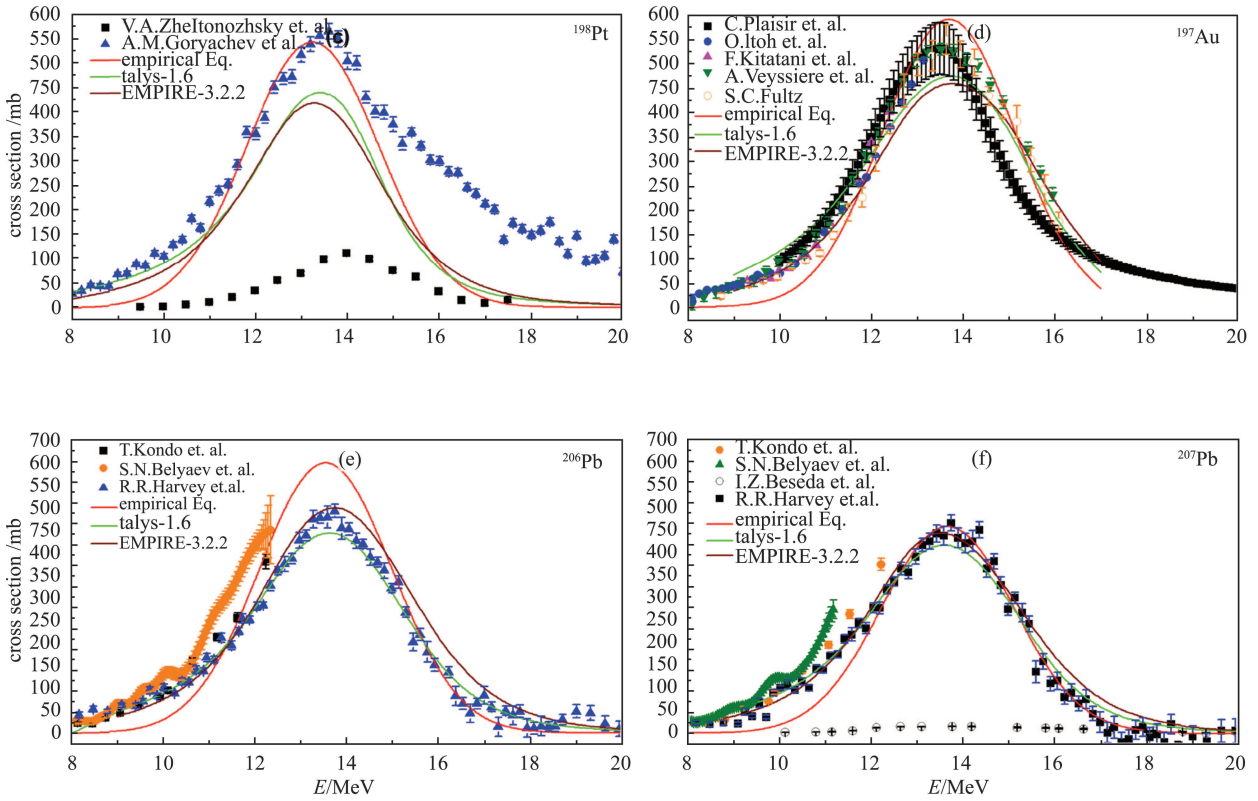


Fig. 9. (color online) Comparison of evaluated data using TALYS-1.6, EMPIRE-3.2.2, and empirical formula with experimental data from EXFOR, for ^{195}Pt , ^{196}Pt , ^{198}Pt , ^{197}Au , ^{206}Pb , and ^{207}Pb .

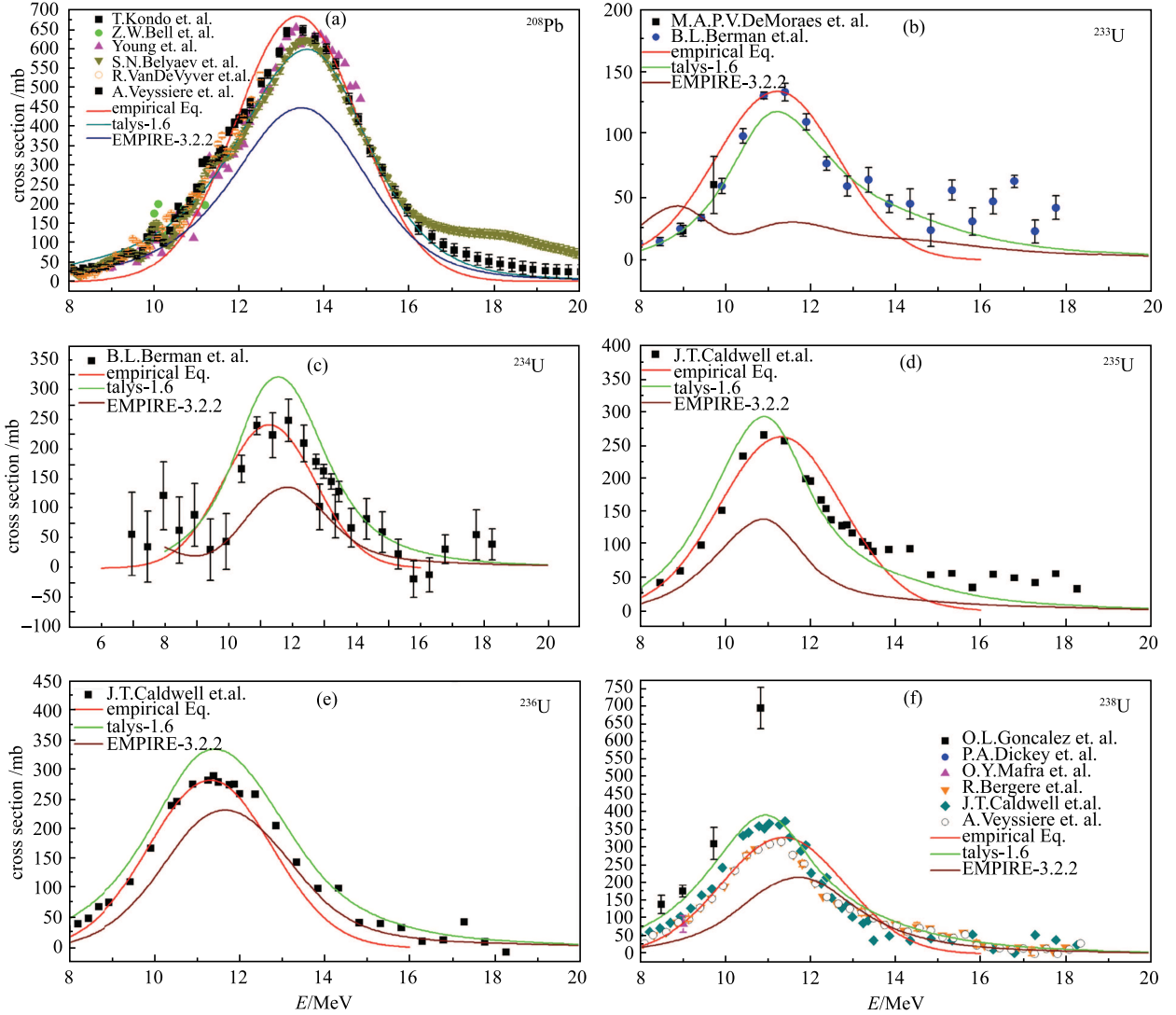


Fig. 10. (color online) Comparison of evaluated data using TALYS-1.6, EMPIRE-3.2.2, and empirical formula with experimental data from EXFOR, for ^{208}Pb , ^{233}U , ^{234}U , ^{235}U , ^{236}U , and ^{238}U .

$$S_{f1} = 1.39 \times S_f, \quad (17)$$

$$S_{f2} = 0.28 \times S_{f1}. \quad (18)$$

The two curves intersect at a deep point, where both curves should have the same value of cross section. This intersection point energy can be calculated by comparing the right-hand side of Eq. (12) for the above values.

$$\begin{aligned} & \sigma_m \cdot e^{-\frac{33.5(N-Z)}{A}} \cdot e^{-\left(\frac{E_i - S_j \cdot R_{p1}}{2}\right)^2} \cdot e^{\sqrt{1+E^{\frac{2}{3}}}} \cdot S_{f1} \\ &= \sigma_m \cdot e^{-\frac{33.5(N-Z)}{A}} \cdot e^{-\left(\frac{E_i - S_j \cdot R_{p2}}{2}\right)^2} \cdot e^{\sqrt{1+E^{\frac{2}{3}}}} \cdot S_{f2}. \end{aligned} \quad (19)$$

Solving this equation, we get

$$E_{\text{deep}} = \frac{1}{2} S_j \cdot (R_{p1} + R_{p2}) + \frac{2 \ln\left(\frac{S_{f2}}{S_{f1}}\right)}{S_j (R_{p1} - R_{p2})}. \quad (20)$$

This energy E_{deep} is near the threshold energy of the $(\gamma, 2n)$ reaction. With this consideration the results are plotted in Fig. 11(a-f).

5 Applications

The (γ, n) cross section for several isotopes of W, Pb, Pa, U and Pu, which have no available experimental data, are calculated and presented using TALYS – 1.6, EMPIRE – 3.2.2 and the present empirical formula. Further, the predicted data of the isotopes were compared with different standard evaluated data libraries, wherever available.

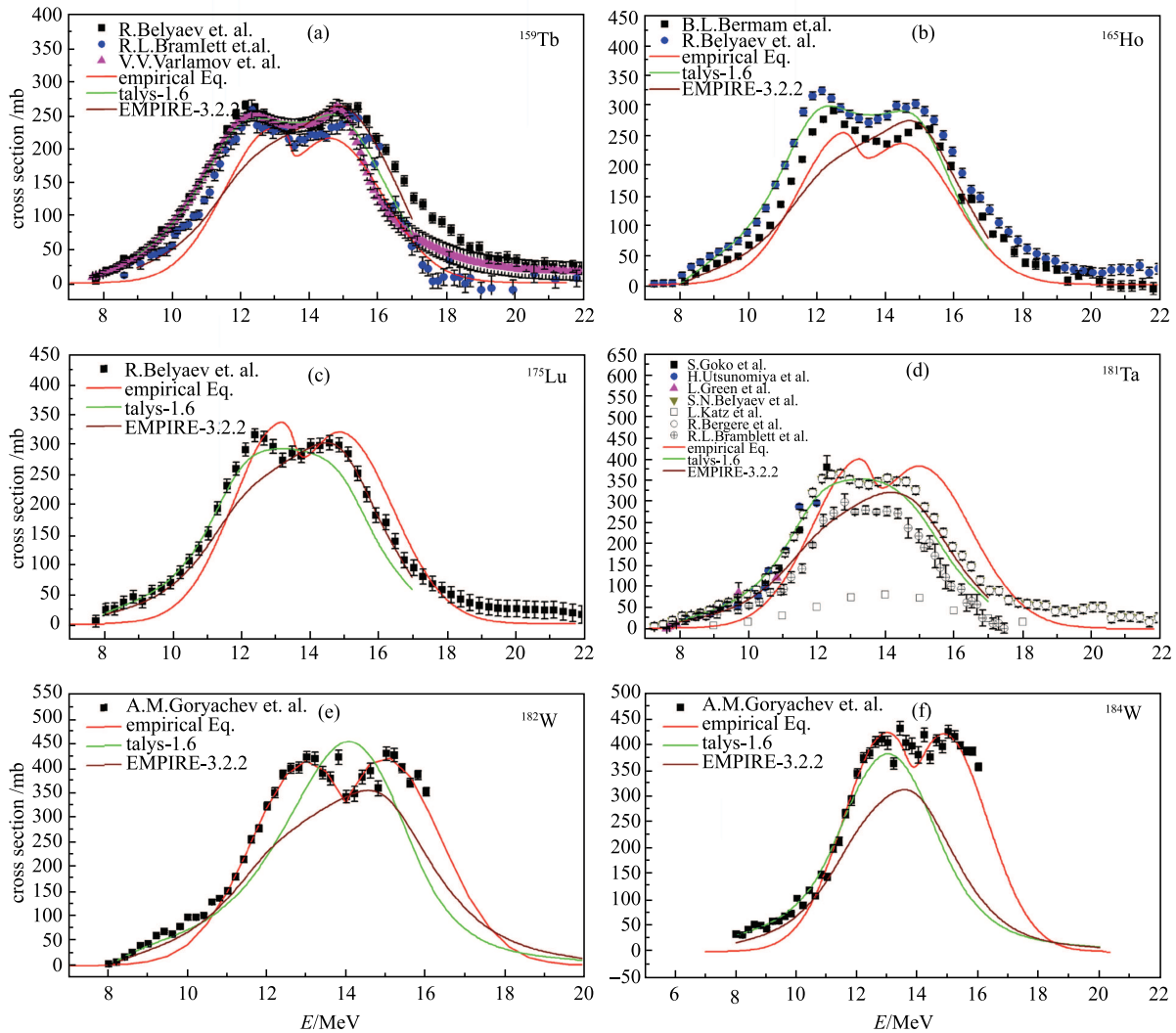


Fig. 11. (color online) Effect of deformed nuclei in (γ, n) nuclear reaction, data comparisons for TALYS – 1.6, EMPIRE – 3.2.2 and present empirical formula.

Tungsten is a prime candidate for the plasma facing component in a fusion reactor. It is selected for the divertor material in the ITER fusion reactor [4]. Tungsten isotopes ^{182}W , ^{184}W and ^{186}W have available experimental data for the (γ, n) reaction cross section [28]. The (γ, n) cross section for the remaining isotopes ^{180}W (0.12%) and ^{183}W (14.31%) are calculated and compared with the evaluated data available in ENDF/B-VII.1. No other standard data library has photonuclear data for these tungsten isotopes [18]. There is an agreement between the present evaluated data and ENDF/B-VII.1, as can be seen in Fig. 12 (a – b) data. Lead is a prime element of the Pb-Li blanket module of fusion reactors, as well as a candidate for the ADS target material [29]. Lead isotopes ^{206}Pb , ^{207}Pb and ^{208}Pb have available experimental data. The (γ, n) cross section for the remaining

isotopes of lead ^{202}Pb (5.25×10^4 y, [30]), ^{203}Pb (51.92 h, [30]), ^{204}Pb (1.4×10^{17} y, [30]) and ^{205}Pb (1.73×10^7 y, [30]) are calculated and presented. These isotopes of lead have large half-lives and they face high energy photons during the runaway electron generation and the disruption phase in plasma [5]. Some isotopes of Pa and U, ^{231}Pa (3.27×10^4 y, [30]), ^{232}U (68.9 y, [30]) and ^{237}U (6.75 d, [30]), with no evaluated cross section data available in different standard data libraries such as ENDF/B-VII.1, JENDL-4.0, JEFF-3.1, ROSFOND and CENDL-3.1 [31, 32], are also calculated and presented here. The evaluated data for ^{239}Pu (2.41×10^4 y, [30]) and available data in ENDF/B-VII.1 are presented in Fig. 13(d). Though in present context, the cross sections are evaluated for limited isotopes, it can be applied to calculate (γ, n) reaction cross sections for actinides using the nuclear

modular codes and present empirical formula. Further, the TALYS - 1.6 and EMPIRE - 3.2.2 codes can be used to calculate the (γ, n) reaction cross section for isotopes which have available GDR parameters, whereas the present empirical formula can be used to calculate cross section for any isotope with $Z \geq 60$.

Another important application is that, by using the nuclear modular codes and the present formula, it is possible to calculate the incident gamma energy for which

the cross section will have its maximum value, i.e. the GDR peak energy. It can be used to calculate the incident charged particle (e.g. electron) beam energy for bremsstrahlung production, which is required to design a photo neutron source. There are some theoretical transport codes available to for electrons and photons, such as MCNP [12, 33, 34], FLUKA [35, 36], GEANT [37] etc. With these codes, one can estimate the bremsstrahlung spectra from the electron beam.

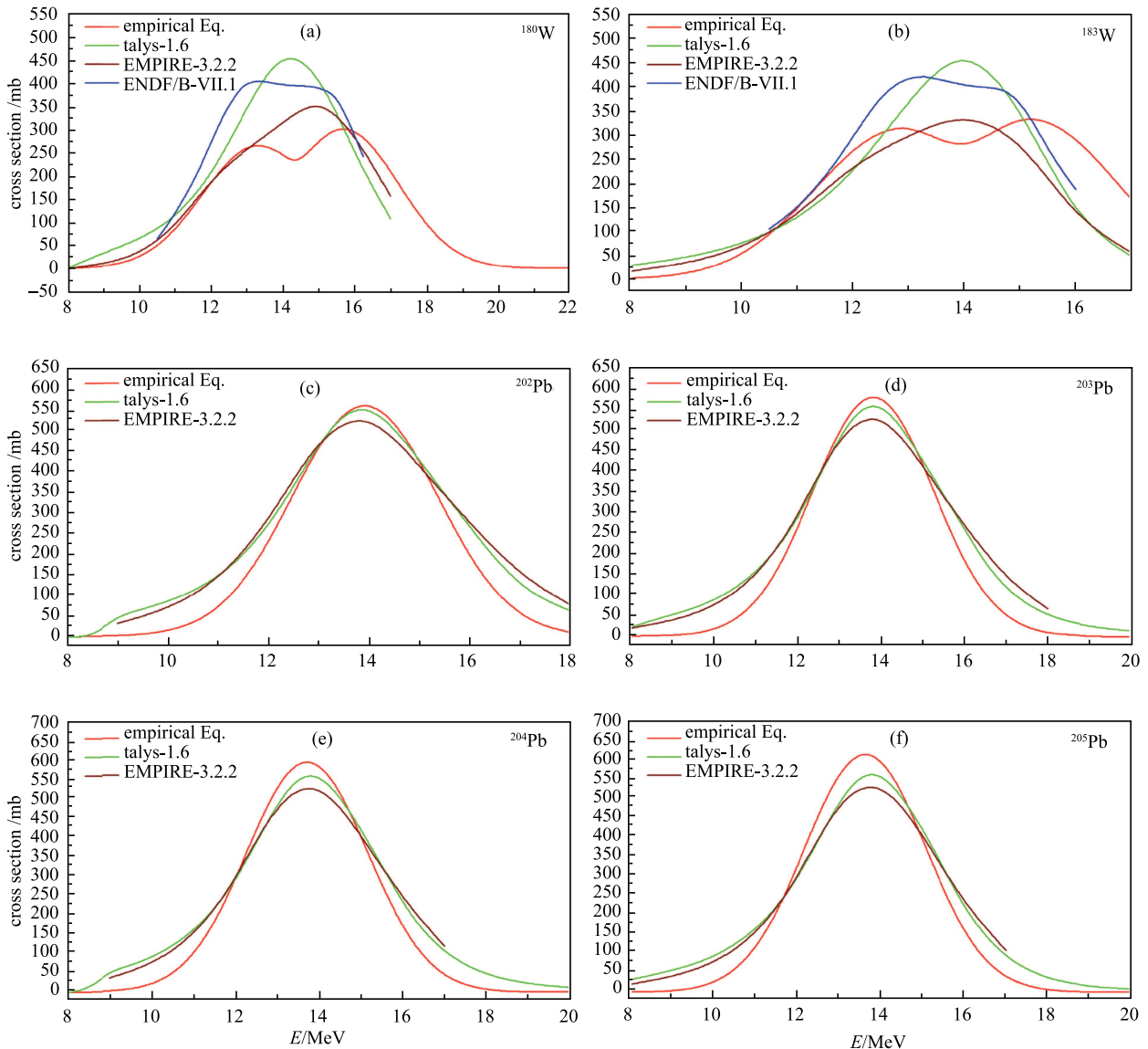


Fig. 12. (color online) Comparison of evaluated data for ^{180}W , ^{183}W , ^{202}Pb , ^{203}Pb , ^{204}Pb , ^{205}Pb using TALYS -1.6, EMPIRE- 3.2.2, and empirical formula.

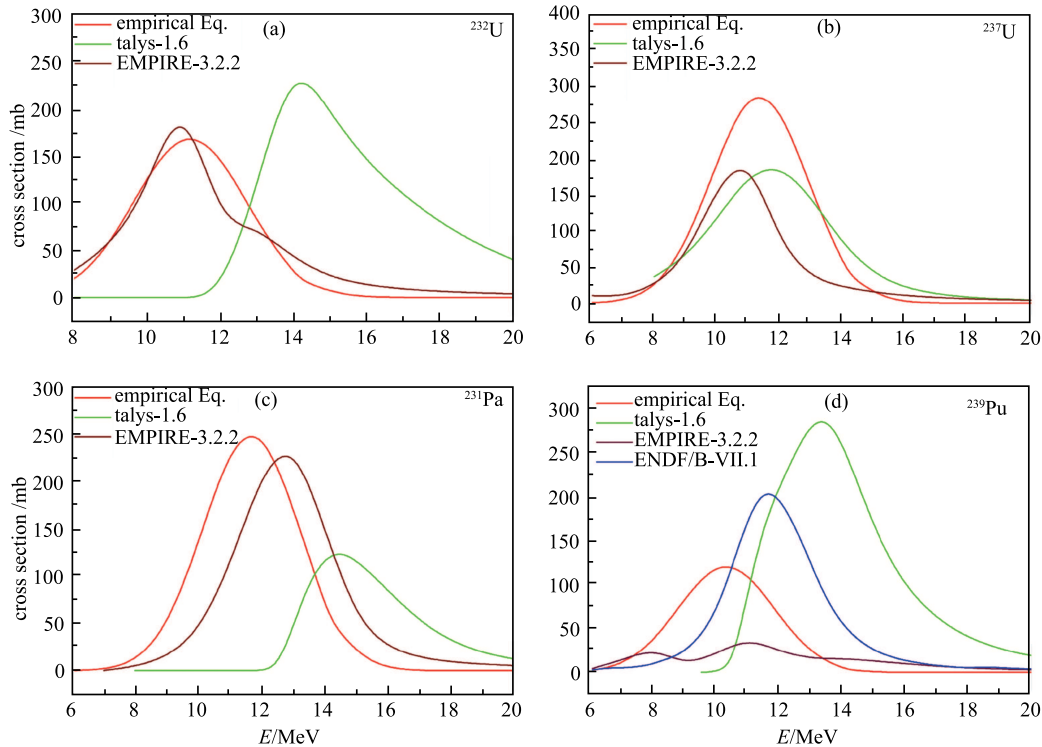


Fig. 13. (color online) Comparison of evaluated data for ^{231}Pa , ^{232}U , ^{237}U , ^{239}Pu using TALYS -1.6, EMPIRE-3.2.2, and empirical formula.

6 Conclusion

In the present work, a new empirical formula has been developed to investigate the (γ, n) reaction cross section for different isotopes with $Z \geq 60$ in the GDR energy region. The results for the (γ, n) reaction cross section obtained by using the above empirical formula have been reproduced by using the nuclear modular codes TALYS - 1.6 and EMPIRE - 3.2.2. It has been shown that TALYS - 1.6, EMPIRE - 3.2.2 and our empirical formula are in agreement with the experimental data. Further a conclusion may be drawn that there may be no deformation in the GDR peak of a pure (γ, n) reaction cross section for spherical nuclei. As a result of the quadrupole, which is due to the asymmetric shape of the nucleus, the present deformation has been observed.

In addition to this, the evaluated data for ^{180}W , ^{183}W , ^{202}Pb , ^{203}Pb , ^{204}Pb , ^{205}Pb , ^{231}Pa , ^{232}U , ^{237}U and ^{239}Pu using TALYS - 1.6, EMPIRE - 3.2.2 and our empirical

formula have been presented. Among these only ^{180}W , ^{183}W and ^{239}Pu have evaluated data in ENDF/B-VII.1 [29], which are compared with the present evaluated data. For ^{180}W and ^{183}W , the present evaluated data are in good agreement, but in the case of ^{239}Pu , it is in disagreement. It is necessary to do experiments in the GDR energy range to validate the present evaluated data for ^{239}Pu . Further, though here only limited isotopes have been used for the (γ, n) reaction cross section evaluation, the empirical formula used in this paper may be useful for other isotopes provided $Z \geq 60$.

Intensive discussions with M. Herman (NNDC, Brookhaven National Laboratory, USA), R. Kapote (NAPC-Nuclear Data Section, IAEA, Austria), P. K. Mehta (The M. S. University of Baroda, Vadodara), P. Mishra (The M. S. University of Baroda, Vadodara), and N. Agrawal (The M. S. University of Baroda, Vadodara) are gratefully to acknowledged.

References

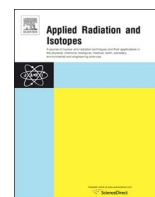
- 1 http://www-pub.iaea.org/MTCD/publications/PDF/te_1178_prn.pdf, retrieved 16th May 2016
- 2 A.R. Junghans et al, Phys. Lett. B, **670**: 200 (2008)
- 3 S. J. Zweben, H. Knoepfel, Phys. Rev. Lett., **35**: 1340 (1975)
- 4 R. A. Pitts et al, Journal of Nuclear Materials, **463**: 39–48 (2013)
- 5 A. Shevelev et al, doi: 10.1063/1.4894038, retrieved 17th May 2016

- 6 B. L. Berman et al, Phys. Rev., **162**: 1098 (1967)
- 7 C. H. M. Broeders et al, Nucl. Eng. Des., **202**: 157 (2000)
- 8 F. R. Allum et al, Nucl. Phys. A, **53** 645 (1964)
- 9 H. Naik et al, Nucl. Phys. A, **916**: 168–182 (2013)
- 10 I. Raškinyteĭ et al, in Proc. Int. Conf. on Nuclear Reaction Mechanisms, (Varenna, Italy: Dapnia/SPhN, 2006), DAPNIA-06-147
- 11 G. Kim et al, Nucl. Instrum. Methods Phys. Res., Sect. A, **485**: 458–467 (2002)
- 12 V. C. Petwal et al, PRAMANA — journal of physics, **68**: 235 (2007)
- 13 M. Gallardo et al, Phys. Lett. B, **191**: 222–226 (1987)
- 14 M. Mattiuzzi et al, Phys. Lett. B, **364**: 13–18 (1995)
- 15 P. Heckman et al, Phys. Lett. B, **555**: 43 (2003)
- 16 Balaram Dey et al, Phys. Lett. B, **731**: 92–96 (2014)
- 17 H. Steinwedel et al, Z. Naturforsch., **5a**: 413 (1950)
- 18 B. L. Berman, At. Data Nucl. Data Tables, **15**: 319–390 (1975)
- 19 G. Reffo, Phys. Rev. C, **44**, 814 (1991)
- 20 S. Levinger, Phys. Rev., **84**: 43 (1951)
- 21 J. S. Levinger, in Nuclear Photo Disintegration (Oxford University Press, Oxford, 1960) p.54
- 22 A. Koning et al, TALYS – 1.6 A nuclear reaction program, (2013) p.62
- 23 M. Herman et al, EMPIRE – 3.2 Malta modular system for nuclear reaction calculations and nuclear data evaluation, (2013) p.18–20
- 24 M. Danos, Nucl. Phys., **5**: 23 (1958)
- 25 T. Belgya et al, Handbook For Calculations of Nuclear Reaction Data, (IAEA, Vienna, RIPL-2,IAEA-TECDOC-1506, 2006), <http://www-nds.iaea.org/RIPL-2>
- 26 V.N. Levkovski, J. Phys., **18**: 361 (1974)
- 27 J. S. Wang et al, Eur. Phys. J. A, **7**: 355–360 (2000)
- 28 <https://www-nds.iaea.org/exfor/exfor.htm>, retrieved 4th December 2015
- 29 Akito Takahashi et al, Fusion Engineering and Design, **9**: 323 (1989)
- 30 <http://www.nndc.bnl.gov/chart/chartNuc.jsp>, retrieved 2nd November 2015
- 31 <https://www-nds.iaea.org/photonuclear/>, retrieved 4th December 2015
- 32 <http://www.nndc.bnl.gov/sigma/index.jsp?dontshow=nn.6&as=9&lib=jendl3.3&nsb=20040>, retrieved 4th December 2015
- 33 Grady Hughes, Progress in Nuclear Science and Technology, **4**: 454–458 (2014)
- 34 X-5 Monte Carlo Team, MCNP-A General Monte Carlo N-Particle Transport Code, Version 5, (2000) 1
- 35 A. Fassò et al, Advanced Monte Carlo for Radiation Physics, Particle Transport Simulation and Applications, in Proceedings of the Monte Carlo 2000 Conference, edited by A. Kling, et. al., (Lisbon, 2000) 159–164
- 36 P. K. Sahani et al, Indian J. Pure Appl. Phys., **50**: 863–866 (2012)
- 37 Boubaker Askri, Nucl. Instrum. Methods Phys. Res., Sect. B, **360**: 1–8 (2015)



Contents lists available at ScienceDirect

Applied Radiation and Isotopes

journal homepage: www.elsevier.com/locate/apradiso

Spectrum average cross section measurement of $^{183}\text{W}(n, p)^{183}\text{Ta}$ and $^{184}\text{W}(n, p)^{184}\text{Ta}$ reaction cross section in $^{252}\text{Cf}(\text{sf})$ neutron field



Rajnikant Makwana^{a,*}, S. Mukherjee^a, L. Snoj^b, S. S. Barala^c, M. Mehta^d, P. Mishra^a, S. Tivari^d, M. Abhangi^d, S. Khirwadkar^d, H. Naik^e

^a Department of Physics, The Maharaja Sayajrao University of Baroda, Vadodara 390002, India

^b Jožef Stefan Institute, Jamova cesta 39, SI-1000 Ljubljana, Slovenia

^c Defence Laboratory, Jodhpur, Rajasthan 342011, India

^d Institute for Plasma Research, Gandhinagar, Gujarat 382428, India

^e Radiochemistry Division, Bhabha Atomic Research Centre, Mumbai 400085, India

HIGHLIGHTS

- The present work describes the measurement of (n, p) reaction cross sections in Cf(sf) neutron field.
- It contains the different corrections using simulation techniques using Monte Carlo based MCNP codes.
- The measurements are on W isotopes which is a very important material for the case of Fusion reactor.
- The (n,p) reaction cross sections are important for the validation of nuclear models.

ABSTRACT

Neutron induced nuclear reactions are of prime importance for both fusion and fission nuclear reactor technology. Present work describes the first time measurement of spectrum average cross section of nuclear reactions $^{183}\text{W}(n, p)^{183}\text{Ta}$ and $^{184}\text{W}(n, p)^{184}\text{Ta}$ using ^{252}Cf spontaneous fission neutron source. Standard neutron activation analysis (NAA) technique was used. The neutron spectra were calculated using Monte Carlo N Particle Code (MCNP). The effects of self-shielding and back scattering were taken into account by optimizing the detector modeling. These effects along with efficiency of detector were corrected for volume sample in the actual source-detector geometry. The measured data were compared with the previously measured data available in Exchange Format (EXFOR) data base and evaluated data using EMPIRE – 3.2.2.

1. Introduction

In the recent decades, there is an overwhelming demand of nuclear reaction cross section data compilation for the development of reactor science and technology. In reactors like International Thermonuclear Experimental Reactor (ITER), fusion reaction process can be studied using the DT reaction. It produces neutrons with energy of 14.1 MeV, and these neutrons are transmitted through the first wall of the reactor material (Qing et al., 2009; Reijonen et al., 2005; Wu et al., 2009; Voitsenya, 2001; De Temmerman et al., 2007; Behringer, 1987). First wall, divertor, blanket and shielding are the main parts of the fusion reactor. First wall, divertor and blanket are directly exposed to the DT plasma and bear the maximum amount of the neutron flux ($\sim 10^{15}$ n/cm²/s). Divertor collects and exhausts heat and particles, and the

reactor walls scatter these neutrons from 14 MeV to the thermal neutron energy. Tungsten has been selected as divertor material for ITER (Lehnen et al., 2013). It will face all the neutron energies from thermal to 14 MeV. These neutrons can open reaction channels such as (n, γ), (n, p), (n, 2n), (n, d), (n, α) etc. It is necessary to have complete nuclear reaction cross section data for the different isotopes of tungsten i.e., $^{183,184,186}\text{W}$, as they can produce different radio isotopes in the reactor (Forrest, 2011). It is very important as a part of reactor maintenance using remote handling.

The reactions $^{183}\text{W}(n, p)^{183}\text{Ta}$ and $^{184}\text{W}(n, p)^{184}\text{Ta}$ are considered here for the cross section measurement using the ^{252}Cf spontaneous neutron source. This is the first time measurement of spectrum average cross section in $^{252}\text{Cf}(\text{sf})$ neutron field. There are plenty of experimental data available at 14 MeV for these reactions; however, very few

* Corresponding author.

E-mail addresses: rajniipr@gmail.com (R. Makwana), sk.mukherjee-phy@msubaroda.ac.in (S. Mukherjee).

measured data are available for energy range from thermal to 14 MeV. Cross sections at low energy are relatively very important as the material tungsten is used in ITER (Forrest, 2011), where the neutron flux will be very high (almost facing $\sim 10^{15}$ neutrons/sec-cm² first wall), the production of the daughter isotope will be expected high amount. Further, there are very few measurements are available and the cross sections are small for these (n, p) reactions, it is necessary to measure cross sections for these reaction with accuracy in order to predict the accurate production of the radioactive waste. Present work describes measurement of cross section for such nuclear reactions. Therefore, the objective of the present work is to have accurate measurements of the cross section of the above mentioned reactions. Further the measured data are important to validate evaluated data libraries for tungsten isotopes from different national projects e.g., ENDF-B/VII.1 (Chadwick et al., 2011), JENDL-4 (Shibata et al., 2011), FENDL (FENDL-3.1 data library, <<https://www-nds.iaea.org/fendl31/>>.), ROSFOND (ROSFOND data library, <<http://www.ippe.ru/podr/abbn/english/libr/rosfond.php>>.), CENDL-3.1 (Ge et al., AugustA 2011), JEFF-3.2 (JEFF-3.2 data library, <https://www.oecd-nea.org/dbforms/data/eva/evatapes/jeff_32/>.) etc.

2. Experimental measurement

The ²⁵²Cf(sf) neutron field is a reference neutron spectra which is considered to be very well known. Mannhart evaluation (Mannhart, 1987; Mannhart, 1989) is currently accepted to be best representation of this reference neutron spectra. Numerical data for this evaluated spectra are available from the IAEA IRDF web page of IAEA (IRDF-, 2002). The average neutron energy in the ²⁵²Cf spectrum is 2.124 MeV. The ²⁵²Cf isotope is an intense neutron emitter that decays by alpha emission (~ 96.31%) and spontaneous fission (~ 3.09%) with half-life of 2.645 y. Its neutron emission rate is 2.314×10^6 n/s/μg (Manojlović et al., 2015). This source is shielded with paraffin, borated wax and lead as shown in Fig. 1.

Standard neutron activation analysis technique was used in the present measurements. In this method a sample with proper weight is required for the irradiation, which is necessary to produce the desired isotope for the measurement of nuclear reaction cross section. The irradiation of W sample was done by using the portable ²⁵²Cf neutron source available at the Defence Laboratory, Jodhpur, India, having present neutron yield of 1.6064×10^8 n/s. The tungsten sample with purity of 99.97% was kept at distance of 60 mm from the ²⁵²Cf neutron source. The sample chosen for irradiation was having a dimension of 8 mm × 8 mm × 5 mm and weighing 6.033 gm. The sample was kept for 603.25 h for continuous long irradiation. The averaged neutron spectrum inside the sample was calculated using the Monte Carlo N Particle Code (MCNP), which is discussed in the next section. The

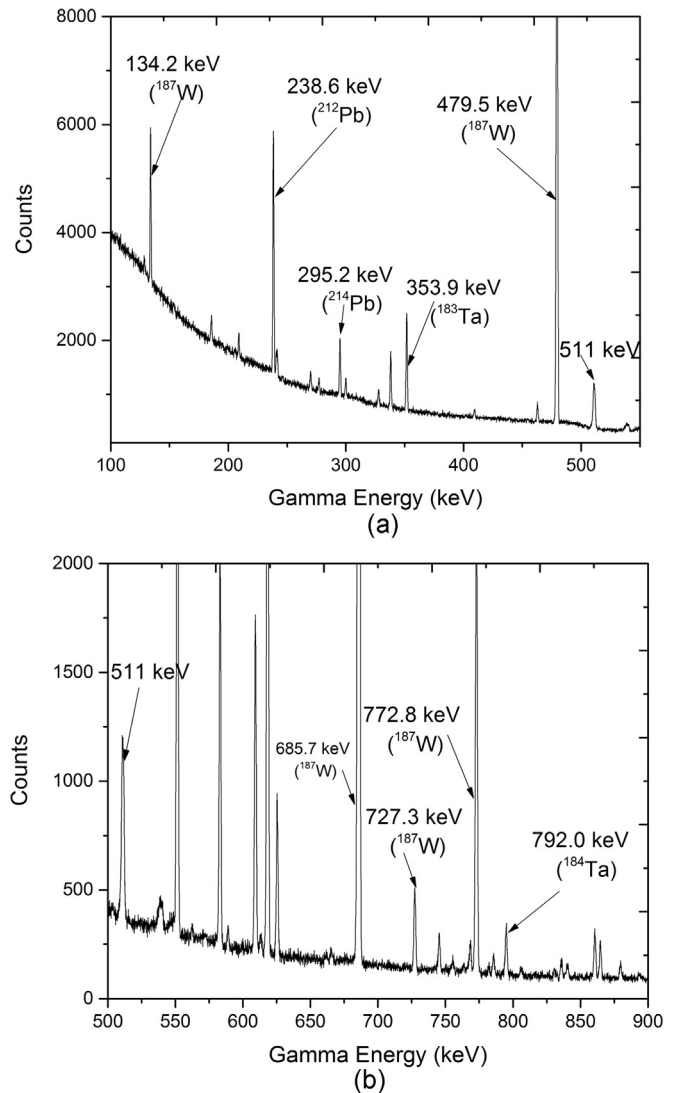


Fig. 2. (a). Gamma spectrum measured using HPGe detector (b). Gamma spectrum measured using HPGe detector.

sample was brought to the Neutronics Laboratory, Institute for Plasma Research (IPR), Gandhinagar, India, for counting purpose. The activated sample was kept near the window of the HPGe detector. Counting was done in two different phases; one was just after irradiation and next

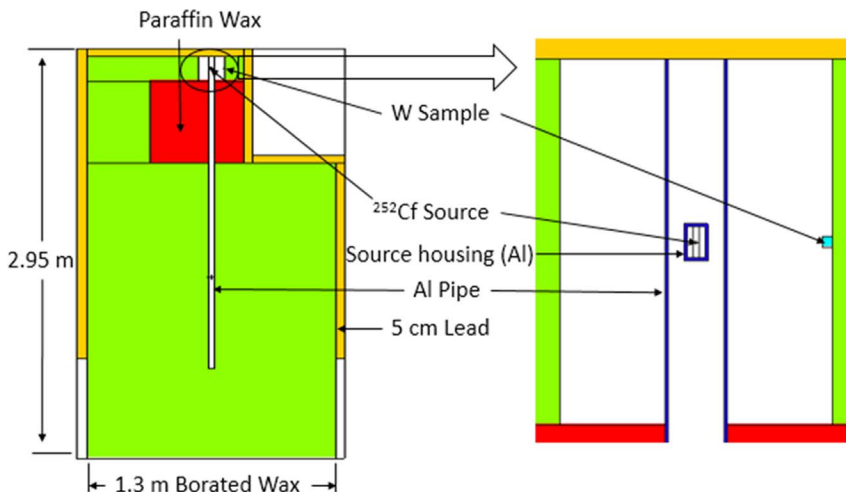


Fig. 1. MCNP modeling of the irradiation experimental setup.

after 2 days cooling. The time of counting was sufficiently long, as the daughter isotopes have half-life from few hours to few days. The gamma spectra measured from the irradiated sample are shown in Fig. 2(a–b). Analysis of the data was done by Neutron Activation Analysis (NAA) technique and cross sections for $^{183}\text{W}(n, p)^{183}\text{Ta}$ and $^{184}\text{W}(n, p)^{184}\text{Ta}$ reactions were estimated.

3. Theoretical calculations using MCNP

This section is divided into two parts, one is regarding the averaged neutron spectra calculation in the irradiated sample, and other is related to detector efficiency. The MCNP-6.1 code was used to perform these calculations. This code has been widely used for transport of neutron, photon, electron and many other particles. All calculations were performed with ENDF/B-VI cross section data library which comes along with MCNP package. Further calculations were checked with ENDF/B-VII, in order to find the difference in results, but no significant change was observed in results.

3.1. Neutron spectra calculation

The ^{252}Cf source is having continuous neutron spectrum, therefore it was necessary to calculate the averaged neutron spectrum inside the sample. The ^{252}Cf was modeled using the MCNP code, as explained by Snoj et al. (Narayan et al., 2010). The most rigorous approach as explained by Snoj et al. is to use evaluated neutron spectrum of Mannhart ((IRDF-, 2002) (Mannhart, 1987, 1989; IRDF-, 2002; [20]NT: IAEA, International reactor dosimetry file 2002 (IRDF-2002) Technical Report Series, International Atomic Energy Agency, Vienna (2006) 162.IAEA, International reactor dosimetry file 2002 (IRDF-2002) Technical Report Series, International Atomic Energy Agency, Vienna (2006) 162.)). In the present work, the average neutron spectra over sample volume have been calculated by using the IRDF – 2002 ^{252}Cf spontaneous fission neutron spectra. Monte Carlo based MCNP code (MCNP – 6.1) with ENDF/B-VII data library was used to model the irradiation assembly as shown in Fig. 1. The tally F4, which gives volume averaged flux tally was used for the calculation. The definition of the F4 tally is represented by following relation.

$$F4 = \frac{1}{V} \int_V dV \int_E dE \int_{4\pi} d\Omega \phi(r, E, \Omega)$$

where, V = volume of the sample, E = energy of the neutron, Ω = solid angle, r = radial distance from source, ϕ = flux at distance.

The calculated spectra is shown in Fig. 3(a). There has been a significant increment in lower energy neutrons due to scattering from the source shielding. However, the higher energy tail shape remained same as in the pure source spectra.

As the chosen reactions have different threshold energies, not whole neutron spectrum was used to produce the daughter isotopes. Only those neutrons above the threshold energy for both reactions are able to produce the daughter isotopes. Hence the low energy neutrons below the threshold can be removed from the neutron spectra for both the reactions. This gives the effective neutron spectrum for the respective reaction. This is shown in Fig. 3(a–c). It can be seen from Fig. 3(a), that the whole neutron spectrum contains very large contribution of low energy (thermalized) neutrons, which are back scattered neutrons from the surrounding shielding materials. As our chosen reactions have threshold above this neutron energies, they do not interfere. The effective neutrons spectra are shown for both reactions in Fig. 3(b,c). Again there is very small number of neutrons is available above 4.5 MeV neutrons. The ratio of these neutrons to total neutrons is $< 6\%$. So the major contribution in the reaction product is due to the neutrons from threshold to 4.5 MeV neutrons. Therefore the measure cross section can be reported at the spectrum averaged energy for these neutrons. Following formula has been used to calculate the spectrum averaged energy from the calculated neutron spectra in the irradiated

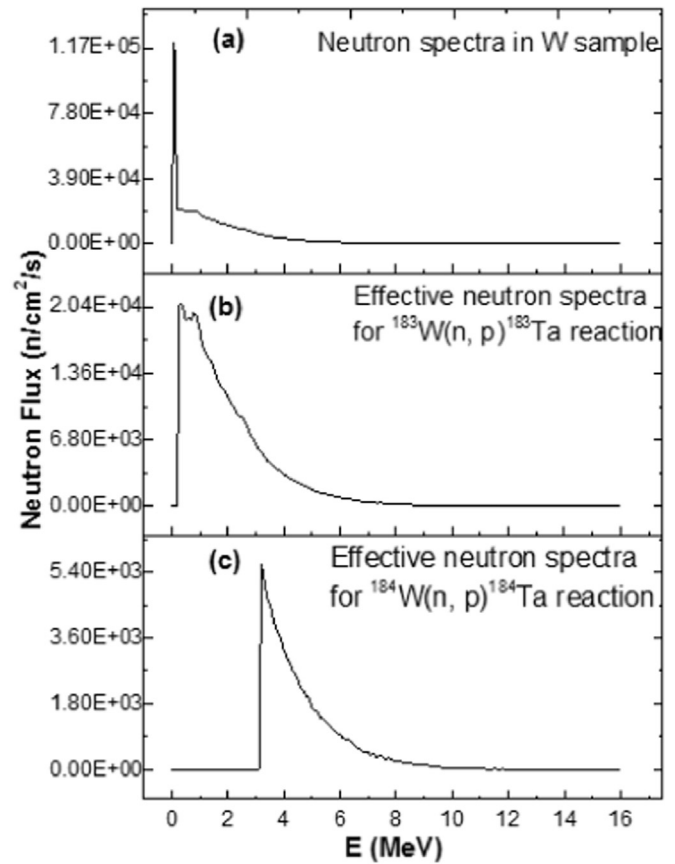


Fig. 3. (a,b,c). Average neutron spectra in W sample, and the effective neutrons above the threshold energy of the selected reactions, calculated using evaluated ^{252}Cf spectra (Koning and Declaroche, 2003; Hauser and Feshbach, 1952) as input source spectra in MCNP.

sample, which is known as the **effective mean energy/spectrum averaged energy** as given below (Smith).

$$E_{\text{mean}} = \frac{\int_{E_{\text{th}}}^{E_{\text{max}}} E_i \phi_i dE}{\int_{E_{\text{th}}}^{E_{\text{max}}} \phi_i dE}$$

In the above expression, E_{th} = threshold energy of the reaction, E_{max} = maximum neutron energy, E_i = energy bin, ϕ_i = neutron flux of energy bin E_i , E_{mean} = effective mean energy.

3.2. Detector efficiency calibration

The HPGe detector was used for the activation measurement having crystal size of 64.80 mm diameter and 64.60 mm length. The window thickness is 0.60 mm made of carbon composite. Efficiency of the detector was measured for different gamma ray energies using mix-energy gamma source available at IPR, Gandhinagar, India. A mix-energy gamma source is a mixture of different radioactive isotopes, such as ^{241}Am (59.54 keV, 919.19 Bq), ^{109}Cd (88.03 keV, 4.132 kBq), ^{57}Co (122.06, 136.47 keV, 144.85 Bq), ^{139}Ce (165.85 keV, 5.050 kBq), ^{51}Cr (320.08 keV, 0.09 Bq), ^{113}Sn (391.69 keV, 91.06 Bq), ^{85}Sr (514.00 keV, 11.85 Bq), ^{137}Cs (661.65 keV, 1.712 kBq), ^{88}Y (898.03 keV, 152.45 Bq), ^{60}Co (1173.22, 1332.49 keV, 2.183 kBq) and ^{88}Y (1836.05 keV, 152.45 Bq), which covers gamma energy from 59 keV to 1.8 MeV. Full efficiency curve was plotted using measured photo peak efficiency. In the present measurements, a point source was used to measure detector efficiency. However, in the actual experiment the volume sample was used. Therefore, it was necessary to obtain efficiency for the volume source of the sample dimension. Further the volume source attenuates photons from the subsequent layers towards the detector, and, large

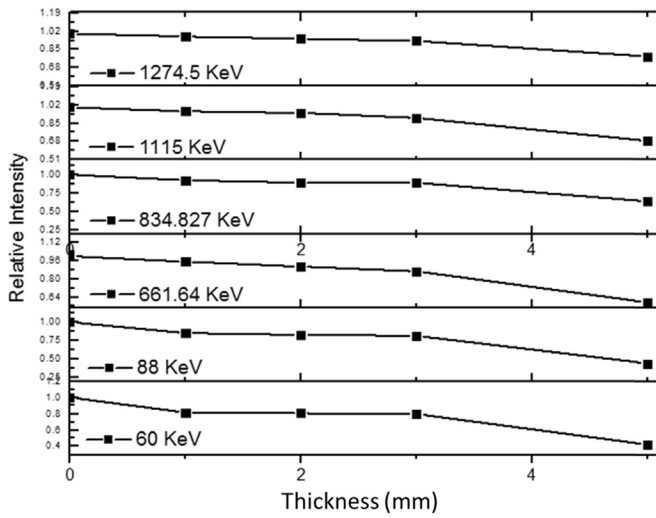


Fig. 4. Relative intensity showing the self-shielding effect increases as the thickness of the sample increases.

number of photons are scattered from the backside layers of the sample. To study the self-shielding and back scattering effect from the W sample, another measurement has been carried out. The method used have been described in reference (Rama Rao et al., 1986). The W samples with the thickness of 1, 2, 3 and 5 mm were kept in between source and detector. In this arrangement the gammas emitted from the source were attenuated by the sample. The results are shown in Fig. 4. It is clear from this figure, that the efficiency will be different for the volume source, due to attenuation. Also the back scattering have significant contribution.

The efficiency of the volume sample by considering back scattering and self-shielding effect can be calculated using the MCNP code. In this context detector was modeled by using this code as shown in Fig. 5. The experimentally measured efficiency at various distances using the point gamma source, at different energies were calculated and compared with simulated efficiency. The model was optimized by getting the ratio Calculated efficiency to Experimental efficiency (C/E ratio) ~ 1, which is shown in Fig. 6(a). The compared results are shown in Fig. 6(b). This model was used for the actual sample – detector geometry to estimate the efficiency of the detector. This method considers both the self-shielding and back scattering effect due to volume of the sample. This efficiency value for different selected gamma energies were used to calculate the cross section using neutron activation technique.

4. Data acquisition and reduction

After the irradiation the target samples were used to measure the gamma activities obtained from the desired isotopes. A typical gamma spectrum obtained from the activated target samples are shown in Fig. 2(a-b). The time of counting were chosen carefully to get the selected gamma energy peaks.

The time elapsed between end of irradiation and start of counting is

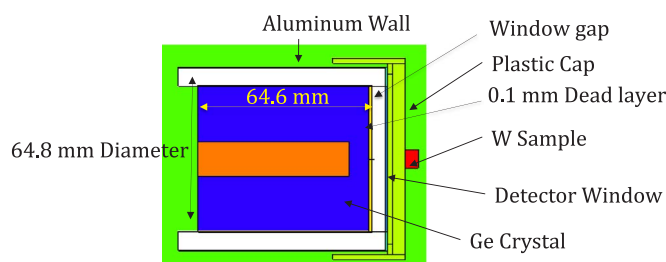


Fig. 5. MCNP Model of the detector to calculate efficiency for irradiated volume sample placed on end cap of the detector.

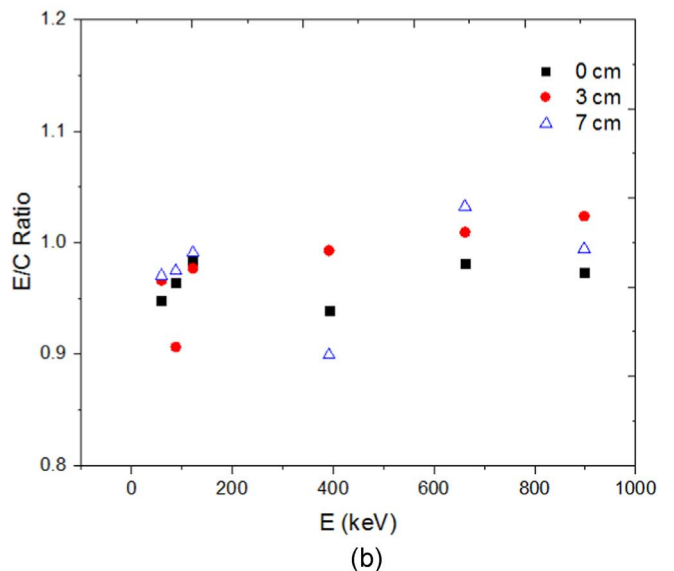
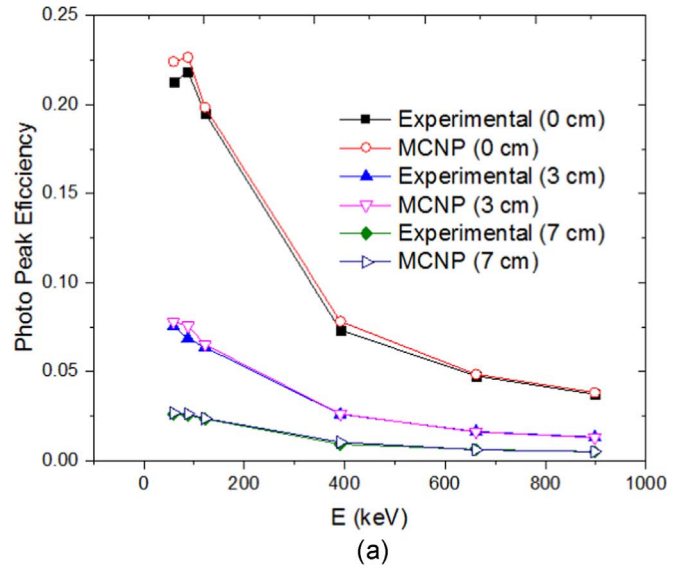


Fig. 6. (a). Comparison of measured and MCNP calculated detector efficiency at various gamma energies (b). Comparison of Experimental to MCNP calculated detector efficiency ratio at various gamma.

known as the cooling time (t_c). The production cross section (σ) of the interested isotope was obtained by using the following standard activation equation,

$$\sigma = \frac{A_I \cdot A_\gamma \cdot \lambda}{(\varnothing \theta_\gamma \epsilon_\gamma w_i P_i N_{av}) \cdot (1 - e^{-\lambda t_i}) \cdot (1 - e^{-\lambda t_c}) \cdot e^{-\lambda t_w}}$$

where, A_I = Gram Atomic Weight of the target; A_γ = Peak Counts of gamma energy; λ = Decay constant of product nucleus (s^{-1}), t_i = irradiation time; t_w = Cooling time; t_c = Counting time; \varnothing = Incident neutron flux; $\theta_\gamma = \gamma$ intensity; ϵ_γ = Efficiency of detector at gamma chosen; w_i = weight of sample (gm), P_i = Abundance of target isotope; N_{av} = Avogadro number.

The photo peak counts of the gamma rays emitted from the desired isotope was carefully measured from the gamma spectrum. The selected gamma energies along with their abundances for the desired radioisotopes are given in Table 1.

5. Nuclear modular code prediction

In order to support the present measured nuclear cross section data,

Table 1

Selected nuclear reactions with isotopic abundance, threshold energy, daughter half-life and daughter gamma energy with its abundance.

Reaction	Abundance of Target Isotope (%) (Rosman and Taylor, 1999)	Threshold Energy (MeV) (Q value calculator, retrieved from: <http://www.nndc.bnl.gov/qcalc/index.jsp>.)	Half life of daughter isotope (Table of Isotopes decay data, retrieved from: <http://nucleardata.nuclear.lu.se/toi/listnuc.asp?Z=74>.)	γ - Energy (KeV)	Γ - Intensity (%) (Table of Isotopes decay data, retrieved from: <http://nucleardata.nuclear.lu.se/toi/listnuc.asp?Z=74>.)
$^{183}\text{W}(n, p)^{183}\text{Ta}$	14.31	0.29	5.1 d	353.9	11.2
$^{184}\text{W}(n, p)^{184}\text{Ta}$	30.64	2.095	8.7 h	792.0	14.2

nuclear modular calculations were performed by using EMPIRE – 3.2.2 code. This code uses different nuclear models to predict nuclear reaction cross section. It can predict nuclear reaction data for neutron, gamma, proton, deuteron, triton, ^3He and alpha with energy range from few keV to several hundreds of MeV. It uses different reaction parameters from RIPL library. It considers effect of level density, and all three nuclear reaction mechanisms: compound, pre-equilibrium and direct reaction. The optical model parameters were obtained by using a global potential proposed by Koning and Delaroche (Koning and Delaroche, 2003). The compound reaction mechanism was incorporated by Hauser-Feshbach model (Hauser and Feshbach, 1952). The pre-equilibrium contribution was included by exciton model, developed by Kalbach (Kalbach, 1986).

In the present case different parameters such as level density parameters were used to evaluate the cross section of the interested nuclear reactions. The EMPIRE – 3.2.2 uses reaction parameters from Reference Input Parameter Library (RIPL) – 3. The calculated reaction cross sections for the production of selected radioisotopes were used to compare the measured reaction cross sections shown Figs. 7 and 8.

6. Results and discussion

The cross sections were measured with improved accuracy, with the application of simulation technique, which incorporates, self-shielding, back scattering, volume source effect in efficiency etc. Geometrical effect and shielding effect on averaged neutron spectra inside the sample was calculated using MCNP simulation. The measured nuclear reaction cross section data are given in Table 2. To the best of our knowledge,

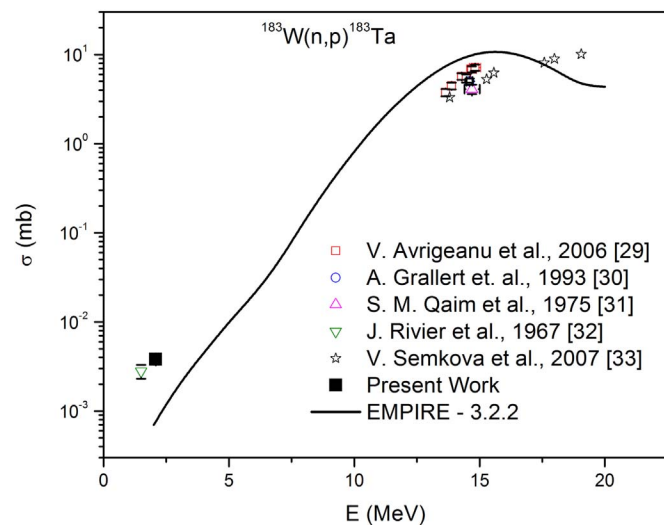


Fig. 7. Comparison of present measured spectrum averaged cross section with experimental data taken from references - Avrigeanu et al. (2006), Grallert et al. (1993), Qaim and Graca (1975), Rivier et al. (1967) and Semkova et al. (2007) and EMPIRE-3.2.2 evaluated cross section for $^{183}\text{W}(n, p)^{183}\text{Ta}$; the present data and data point of Rivier et al. (1967) are spectrum averaged cross sections, other experimental data are for mono energy neutrons.

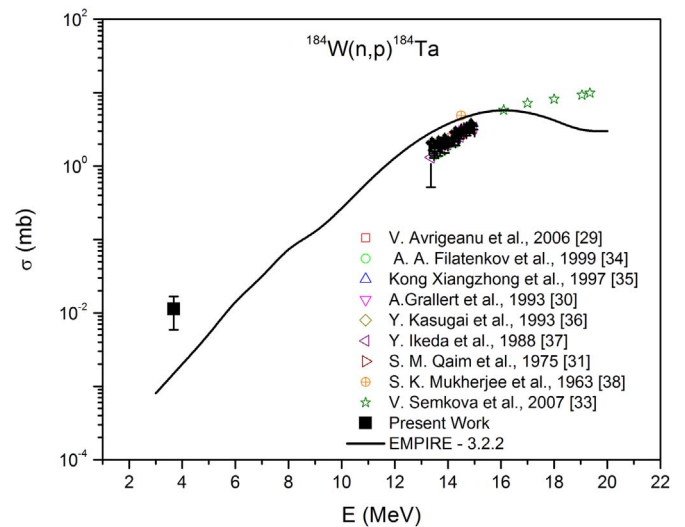


Fig. 8. Comparison of present measured spectrum averaged cross section with experimental data taken from references - Avrigeanu et al. (2006), Reimer et al. (2005), Kong Xiangzhong et al. (1997), Grallert et al. (1993), Kasugai et al. (1992), Ikeda et al. (1988), Qaim and Graca (1975), Gujarathi and Mukherjee (1967) and Semkova et al. (2007) and EMPIRE-3.2.2 evaluated cross section for $^{184}\text{W}(n, p)^{184}\text{Ta}$; the present data and data point of Rivier et al. (1967) are spectrum averaged cross sections, other experimental data are for mono energy neutrons.

Table 2

Measured Cross section for the selected nuclear reactions.

Reaction	Neutron Energy (MeV)	Measured Cross section (mb)
$^{183}\text{W}(n, p)^{183}\text{Ta}$	1.70 ± 1.35	$(3.8 \pm 0.3) \times 10^{-3}$
$^{184}\text{W}(n, p)^{184}\text{Ta}$	3.75 ± 1.26	$(11.3 \pm 0.9) \times 10^{-3}$

the present measurements have been done for the first time in the above mentioned neutron energies. The neutron energy was taken as a spectrum averaged from calculated neutron spectra using MCNP code. The effect of self-attenuation and back scattering, and the sample-volume geometry effect on the efficiency of the detector, was corrected by optimizing MCNP model of the HPGe detector at different distances and for different energies of gamma photon. The parameters for the error propagation in the final cross section estimations were considered. Major error contributions in the present data are due to relative efficiency (2–3%), scattered neutron (1–3%), statistical error (3–4%), detector dead time (< 2%). The overall error in the present measurement were < 6%.

The EMPIRE-3.2.2 nuclear modular code was used for evaluating the cross section of the selected nuclear reactions. The measured data were compared with the evaluated data in the Figs. 7 and 8. In the case of $^{183}\text{W}(n, p)^{183}\text{Ta}$, there is a previous measurement for this reaction near to the present listed energy, by Rivier et al. (Reimer et al., 2005). Although the measurement reported by Rivier et al. (Rosman and Taylor, 1999) was in reactor neutron field it presents cross section value

at spectrum average energy, which are in agreement with the present data. It should be noted that the average energy of a reactor spectrum is very difficult to define, we accept the energy, which Rivier et al. has listed for present reference. In both the (n, p) reactions the measured cross sections are higher by a small factor in comparison with the evaluated data.

7. Conclusions

In the present measurements, cross sections of $^{184}\text{W}(n, p)^{184}\text{Ta}$, and $^{183}\text{W}(n, p)^{183}\text{Ta}$ reactions were measured using a ^{252}Cf neutron source at spectrum averaged energies from threshold of the reaction to the maximum available neutron energy. This is a material of interest for fusion reactor. The averaged neutron spectra inside the sample volume were calculated using MCNP code. The data that have been presented for (n, p) reactions for the available energies, have very few or no previous measurements. The theoretical estimation of the cross section was done by EMPIRE-3.2.2 code. It may be observed that present experimental results are in agreement within the limits of the experimental error. The study shows that the cross section of (n, p) reaction for tungsten isotopes are having small values. But for the case of the fusion reactor, where the first wall is facing $\sim 10^{15}$ neutrons/sec-cm², it can produce considerable amount of radioactive waste.

Acknowledgements

Authors are grateful to Mr. Mahavir from Defence Laboratory, Jodhpur, India, Mr. Naveen Agrawal, The M. S. University of Baroda, Vadodara, and Dr. B. Pandey from Pantanagar University, India for useful suggestions. One of the authors (SM) thanks DAE-BRNS, Government of India, for the sanction of a major research project.

References

- Qing, J., Wu, Y., Regis, M., Kwan, J.W., 2009. IEEE Trans. Nucl. Sci. 56, 1312–1315.
- Reijonen, J., Gicquel, F., Hahto, S.K., King, M., Lou, T.P., Leung, K.N., 2005. Appl. Radiat. Isot. 63, 757–763.
- Wu, Y., Hurley, J.P., Ji, Q., Kwan, J., Leung, K.N., 2009. IEEE Trans. Nucl. Sci. 56, 1306–1311.
- Voitsenya, V., et al., 2001. Rev. Sci. Instrum. 72, 475–482.
- De Temmerman, G., Pitts, R.A., Voitsenya, V.S., Marot, L., Veres, G., Maurer, M., Oelhafen, P., 2007. J. Nucl. Mater. 363, 259–263.
- Behringer, K.H., 1987. J. Nucl. Mater. 145, 145–153.
- Lehnen, M., Aleynikova, K., Aleynikov, P.B., Campbell, D.J., Drewelow, P., Eidielis, N.W., Gasparyan, Yu, Granetz, R.S., Gribov, Y., Hartmann, N., Hollmann, E.M., Izzo, V.A., Jachmich, S., Kim, S.-H., Koc'an, M., Koslowski, H.R., Kovalenko, D., Kruezi, U., Loarte, A., Maruyama, S., Matthews, G.F., Parks, P.B., Pautasso, G., Pitts, R.A., Reux, C., Riccardo, V., Roccella, R., Snipes, J.A., Thornton, A.J., de Vries, P.C., 2013. EFDA JET contributors. J. Nucl. Mater. 463, 39–48.
- Forrest, R.A., 2011. Energy Procedia 7, 540–552.
- Chadwick, M.B., Herman, M., Obložinský, P., Dunn, M.E., Danon, Y., Kahler, A.C., Smith, D.L., Pritychenko, B., Arbanas, G., Arcilla, R., Brewer, R., Brown, D.A., Capote, R., Carlson, A.D., Cho, Y.S., Derrien, H., Guber, K., Hale, G.M., Hoblit, S., Holloway, S., Johnson, T.D., Kawano, T., Kiedrowski, B.C., Kim, H., Kunieda, S., Larson, N.M., Leal, L., Lestone, J.P., Little, R.C., McCutchan, E.A., MacFarlane, R.E., MacInnes, M., Mattoon, C.M., McKnight, R.D., Mughabghab, S.F., Nobre, G.P.A., Palmiotti, G., Palumbo, A., Pigni, M.T., Pronyaev, V.G., Sayer, R.O., Sonzogni, A.A., Summers, N.C., Talou, P., Thompson, I.J., Trkov, A., Vogt, R.L., van der Marck, S.C., Wallner, A., White, M.C., Wiarda, D., Young, P.G., 2011. ENDF/B-VII.1: nuclear data for science and technology: cross Sections, covariances, fission product yields and decay Data. Nucl. Data Sheets 112, 2887.
- Shibata, Keiichi, Iwamoto, Osamu, Nakagawa, Tsuneo, Iwamoto, Nobuyuki, Ichihara, Akira, Kunieda, Satoshi, Chiba, Satoshi, Furutaka, Kazuyoshi, Otuka, Naohiko, Ohasawa, Takaaki, Murata, Toru, Matsunobu, Hiroyuki, Zukeran, Atsushi, So, Kamada Jun-ichi Katakura K., Shibata, e., 2011. J. Nucl. Sci. Technol. 48 (1), 1–30.
- FENDL-3.1 data library, <https://www-nds.iaea.org/fendl31/>.
- ROSFOND data library, <http://www.ippe.ru/podr/abbn/english/libr/rosfond.php>.
- Ge, Z.G., Zhao, Z.X., Xia, H.H., Zhuang, Y.X., Liu, T.J., Jhang, J.S., Wu, H.C., 2011. J. Korean Phys. Soc. 59 (2), 1052.
- JEFF-3.2 data library, <https://www.oecd-nea.org/dbforms/data/eva/evatapex/jeff_32/>.
- Mannhart, W., 1987. IAEA-TECDOC-410 158.
- Mannhart, W., 1989. INDC(NDC)-220/L 305.
- IRDF., 2002. <https://www-nds.iaea.org/IRDF/IRDF-v1-05.sp.endf>.
- Manojlović S., Trkov A., Žerovnik G., Snoj L., 2015. Applied Radiation and Isotopes, 101, pp. 101–106.
- Narayan, Pradeep, Meghwal, L.R., Songara, K.C., Vajjapurkar, S.G., Bhatnagar, P.K., 2010. Indian J. Pure Appl. Phys. 48, 798–801.
- . IAEA, International reactor dosimetry file 2002 (IRDF-2002) Technical Report Series, International Atomic Energy Agency, Vienna (2006) 162.
- Smith, D.L. et al., Corrections for Low Energy Neutrons by Spectral Indexing, Retrieved from: <https://www.oecd-nea.org/science/docs/2005/nsc-wpec-doc2005-357.pdf>.
- Rama Rao, J., Singh, N.L., Singhal, S., Mohan Rao, A.V., Mukherjee, S., Chaturvedi, L., 1986. Nucl. Instrum. Methods Phys. Res., Sect. B 17, 368–371.
- Koning, A.J., Declaroche, J.P., 2003. Nucl. Phys. A 713, 231–310.
- Hauser, W., Feshbach, H., 1952. Phys. Rev. C 87, 366.
- Kalbach, C., 1986. Phys. Rev. C 33, 818–833.
- Rosman, K.J.R., Taylor, P.D.P., 1999. Pure Appl. Chem. 71, 1593–1607.
- Q value calculator, retrieved from: <http://www.nndc.bnl.gov/qcalc/index.jsp>.
- Table of isotopes decay data, retrieved from: <http://nucleardata.nuclear.lu.se/toi/listnuc.asp?Z=74>.
- Avriganu, V., Chuvaev, S.V., Eichin, R., Filatenkov, A.A., Forrest, R.A., Freieslebe, H., Herman, M., Koning, A.J., Seidel, K., 2006. Nucl. Phys. A 765, 1–28.
- Grallert, A., Csikai, J., Buczk, Cs.M., 1993. Rept.: IAEA Nucl. Data Sect. Report. I. N. D. C. No. 286, 131.
- Qaim, S.M., Graca, C., 1975. Nucl. Phys. A 242, 317–322.
- Rivier, J., Blachot, J., Hocquenghem, J.C., 1967. J. Radio Chem. Acta 8, 196.
- Semkova, V., Capote, R., Jaime Tornin, R., Koning, A.J., Moens, A., Plompen, A.J.M., 2007. doi: http://dx.doi.org/10.1051/ndata:07320.
- Reimer, P., Avriganu, V., Chuvaev, S.V., Filatenkov, A.A., Glodariu, T., Koning, A., Plompen, A.J.M., Qaim, S.M., Smith, D.L., Weigmann, H., 2005. Phys. Rev. C 71, 044617.
- Kong Xiangzhong et al., 1997. Rept.: Chinese report to I.N.D.C. No. 042 9.
- Kasugai, Y., Tokushima, T., Kawade, K., Yamamoto, H., Katoh, T., Takahashi, A., Iida, T., 1992. Conference: JAERI-M Report No. 92, 27, 268.
- Ikeda, Y., Konno, C., Oishi, K., Nakamura, T., Miyade, H., Kawade, K., Yamamoto, H., Katoh, T., 1988. JAERI Reports No.1312, 1.
- Gujarathi, S.C., Mukherjee, S.K., 1967. Indian J. Phys. 41, 667.

Measurement of (n,p) Cross Section for Some Structural Materials at 14.2 MeV

Nand Lal Singh, Rajnikant Makwana,
S. Mukherjee, and A. Chatterjee
Department of Physics,
The Maharaja Sayajirao University of Baroda,
Vadodara – 390 002, India
nl.singh-phy@msubaroda.ac.in

Abstract—The (n,p) reaction cross section for some structural materials such as ^{75}As , ^{66}Zn , ^{64}Zn , ^{55}Mn , ^{51}V and ^{58}Ni was measured at 14.2 ± 0.2 MeV using activation and off line gamma ray spectroscopic technique. For the purpose of safe and economical design of reactors, the neutron cross section data for structural materials are required with high precision and accuracy. The neutron cross section data for important structural materials are collected and evaluated systematically and data files are prepared for the reactor design. However, considerably large discrepancies exist among different evaluated nuclear data files. Hence there is a need to study these reactions with better accuracy. The results were compared with existing data available in EXFOR data base. The measured cross sections were also estimated theoretically using nuclear modular codes: TALYS-1.6 and EMPIRE-3.2.2.

Keywords—Activation technique; Structural materials; Neutrons 14 MeV; TALYS-1.6; EMPIRE

I. INTRODUCTION

Accurate knowledge of neutron induced reaction cross sections is of interest to many areas of applied science and fundamental physics. These cross sections are important to estimate radiation levels and decay heat of materials that have been exposed to radiation fields. Other applications are designing of future fusion and advanced fission reactors, in neutron dosimetry and development of nuclear theory. Structural materials are very important part of any reactor. They must have capability of radiation hardness and long durability [1]. As these materials are used for a reactor structure, the neutrons produced from the fission or fusion mechanism of reactor are irradiating them. The D-T fusion reaction will produce high energetic neutrons of 14 MeV. It is necessary to have all the known cross section for this neutron energy to calculate nuclear activation and transmutation, nuclear heating, nuclear damage. The (n, p) reaction channel easily opens for most of the materials above a few MeV of neutron energy. The uncertainties arising due to self-absorption and self-scattering effects in the bulk samples and pile up effect in detector have been taken care by simulation method as discussed in our earlier papers [2]. The following reaction cross section was measured by activation technique: $^{75}\text{As}(n,p)^{75}\text{Ge}$; $^{66}\text{Zn}(n,p)^{66}\text{Cu}$; $^{64}\text{Zn}(n,p)^{64}\text{Cu}$; $^{55}\text{Mn}(n,p)^{55}\text{Cr}$; $^{51}\text{V}(n,p)^{51}\text{Ti}$ and $^{58}\text{Ni}(n,p)^{58}\text{Co}$. The literature survey reveals that the neutron induced reaction cross sections for

these materials are widely studied using standard activation method and are available in EXFOR data base [2]. There is often large discrepancy among the previous experimental data by a factor of 1.4 to 4.0, hence further measurements are required. The measured cross section is important for the fusion reactor as well as for the advance accelerator based sub-critical system. Theoretical evaluation of (n,p) reaction cross sections are done using standard nuclear modular codes, TALYS-1.6 and EMPIRE-3.2.2. The predictive power of nuclear model codes can be validated and improved in comparison with good quality experimental data and in turn the model calculation provide estimates where no experimental data are available.

II. EXPERIMENTAL

A. Sample preparation and efficiency of the detector

The isotope of ^{75}As , ^{66}Zn , ^{64}Zn , ^{55}Mn is in spectrally pure oxide form and pallets of 2.0 cm diameter and thickness of about 2.0 mm each were prepared by mixing uniformly aluminium powder with each isotope. Few pellets were used as a cylindrical experimental target. In the case of nickel and vanadium instead of pellets, the stack of alternative Ni/V and Al foils was used as a target. A ^{152}Eu disc source of same diameter was placed between the pellets at different positions. Gamma spectrum at each position was measured with high resolution HPGe detector (1.8 keV FWHM at 1332 keV gamma energy) and 4096 channel multi-channel analyser. Efficiency of detector was calculated at different energies of ^{152}Eu with and without sample to remove self-absorption and self-scattering effects in the samples and pile up effect in detector as discussed in our earlier papers [2] and is shown in Fig.1 for nickel and zinc oxide. It reveals that the percentage attenuation varies nearly 22% to 2.3% for ZnO and 16% to 1.9% for Ni sample for low energy (122 keV) to high energy (1408 keV) gamma rays respectively.

B. Description of irradiation

The AN-400 Van de Graff Accelerator of Banaras Hindu University, Varanasi, India was used to produce 14 MeV neutron via $^3\text{H}(d,n)^4\text{He}$ reaction using tritium target of 8 Ci activity and deuteron beam of energy 180 keV having a beam current ~ 30 μA . The samples were placed at 0° angle relative

to the beam direction at a distance of about 3.0 cm

These isotopes were irradiated with a flux of the order of 10^7 n/s for 15 min to 4 hours as per the half-life of product produced in the reaction. The reaction products were identified by means of their characteristics gamma rays and half-life as listed in Table-1.

C. Measurement of cross section by gamma spectroscopy

The gamma spectra were measured for each sample using the above mentioned detector setup. The cross section was calculated from the measured photo peak counts using the following activation equation [2].

$$\sigma = \frac{A_i A_\gamma \lambda (e^{-\lambda t_w})}{\phi \theta_\gamma P_\gamma w_i P_i N_{av} (1 - e^{-\lambda t_i}) (1 - e^{-\lambda t_c})} \quad (1)$$

where, σ is the cross section for the reaction (mb), A_i is the gram atomic weight of the target element, A_γ is the area under the photo peak of the characteristic gamma ray of the residual nucleus, λ is the disintegration constant of the product nucleus (s^{-1}), ϕ is the flux of the incident particle (particle s^{-1}), θ_γ is the absolute γ -ray intensity per decay of the residual nucleus, P_γ is the photopeak efficiency of the gamma ray, w_i is the weight per unit area of the target ($g\ cm^{-2}$), P_i is the fractional abundance by weight of the target isotope of interest, N_{av} is the Avogadro number (6.023×10^{23} atoms $mole^{-1}$), t_i is the time duration for irradiation, t_w is the time elapsed between the end of irradiation and start of counting, t_c is the data collection time (or counting time).

TABLE I. SELECTED NUCLEAR REACTIONS

Nuclear Reaction	Q - Value (MeV)	Half-life	Emitted Gamma (keV)	Γ - Abundance
$^{75}As(n,p)^{75}Ge$	- 0.3954	82.78m [4]	264.65	11
			198.60	1.19
$^{66}Zn(n,p)^{66}Cu$	- 1.8592	5.120 m [5]	1039.23	9
$^{64}Zn(n,p)^{64}Cu$	0.2040	12.7 h [7]	1345.84	0.473
$^{55}Mn(n,p)^{55}Cr$	- 1.8213	3.497 m [6]	1528.3	0.037
$^{51}V(n,p)^{51}Ti$	- 1.6837	5.76 m [8]	320.07	93.1
$^{58}Ni(n,p)^{58}Co$	0.4021	70.86 d [9]	511	29.8
			810.76	99.45
Monitor Reactions				
$^{27}Al(n,\alpha)^{24}Na$	- 3.1302	14.96 h	1368.6	100
$^{27}Al(n,p)^{27}Mg$	-1.8269	4.46 m	843.8	71.8

The activities produced in the reaction products of monitor and samples were measured via gamma rays spectrometry. The counting geometry was kept in such a way so that the dead time of detector was about 4%. The average neutron flux was determined from Al-monitor via $^{27}Al(n,p)^{27}Mg$ and $^{27}Al(n,\alpha)^{24}Na$ reactions.

TABLE II. MEASURED CROSS-SECTION DATA

Nuclear Reaction (Half life)	Measured Cross section (mb) 14.2 ± 0.2 MeV	Evaluated Data Cross section (mb)	
		TALYS 1.6	EMPIRE 3.2.2
$^{75}As(n,p)^{75}Ge$	27.2 ± 2.1	25.58	22.44
$^{66}Zn(n,p)^{66}Cu$	55.5 ± 4.4	50.72	49.32
$^{64}Zn(n,p)^{64}Cu$	170.0 ± 13.6	137.12	176.33
$^{55}Mn(n,p)^{55}Cr$	45.8 ± 3.7	26.92	36.23
$^{51}V(n,p)^{51}Ti$	28.2 ± 2.3	35.90	30.52
$^{58}Ni(n,p)^{58}Co$	314.0 ± 25.1	278.96	263.83

D. Results and Discussion

The cross section was measured with improved accuracy using the simulation method, which takes care of self-absorption and self-scattering effects in the samples and pile up effect in detector. The area under the peak of characteristics gamma rays was corrected for self-attenuation effect in the samples and used for cross section calculation. The relative efficiency data with and without absorber for a particular target-detector geometrical arrangement inclusive of all due to self-scattering, self-absorption and geometry solid angle for a simulated cylindrical target was used to determine cross section, such curve for nickel and zinc oxide is presented in Fig.1. The cross section was calculated relative to the standard reactions of monitor as mentioned in the Table 1. For this reason, each sample was thoroughly mixed with aluminum powder and then pellets were made or Al foils were placed alternatively in the case of foil samples. The (n,p) cross section will be affected by the low energy neutrons since reactions have low threshold energies. In addition, the effect of low energy neutrons scattered from the walls of the laboratory and other heavy masses around the target will give rise to inelastically scattered neutrons. In our case the distance of walls from the centre of the target is 521 cm and there is a pit in the floor of diameter 310 cm and depth of 272 cm. Therefore, the contribution from low energy back ground is expected to be small and may be of the order of 3-5% depending on the reaction threshold of the investigated reactions.

The uncertainties quoted on the cross section comprise the statistical error (1-3%), relative efficiency (2-3%), monitor cross section (3%) and neutron scattering (3-5%). The present experimental results are compared with the available experimental data from EXFOR database [4-8] and are shown in Figs.2-7. The cross section measured in the present work

and by others with same experimental method is in agreement within about 2-15%.

III. THEORETICAL PREDICTIONS

The nuclear modular codes are important tool for the calculation and verification of the cross sections of various nuclear reactions at different incident energy of projectile. The latest version of nuclear modular codes TALYS-1.6 and EMPIRE-3.2.2 were used to evaluate (n, p) cross sections for the selected isotopes [10,11]. The input parameters such as level density parameter have been precisely chosen for best estimation of cross section.

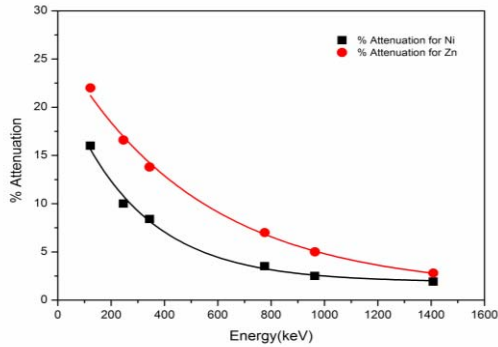


Fig. 1. Self-absorption and self-scattering effect for Ni and Zn sample

A. TALYS-1.6 calculations

TALYS is a computer code which is efficient to predict nuclear reaction cross section. It is useful tool to do analysis of physics of nuclear reactions. TALYS-1.6 nuclear code can calculate cross section for incident particles; gammas, neutrons, protons, deuterons, tritons, ^3He and alpha-particles in the incident energy range from 1 keV to 200 MeV for target nuclides of mass 12 and heavier nuclei. TALYS considers all the possible channels for the above-mentioned particles. It has completely integrated optical model and coupled-channels calculations by ECIS-06 code [12]. Talys-1.6 is the most advance version of all the version of the TALYS code. The optical model parameters are used for neutron and photon reaction calculations determined from global potential proposed by Koning and Delaroche [13]. The compound model contribution is developed from Hauser-Feshbach model [14]. The pre-equilibrium calculation is developed from the exciton model proposed by Kalbach [15]. In this calculation, pre-equilibrium effect was also considered.

B. EMPIRE-3.2 calculations

EMPIRE-3.2 is another powerful nuclear modular system to predict nuclear reaction cross section. It considers reaction mechanism such as compound nucleus formation (Hauser-Feshbach model with width fluctuation correction [14, 16], pre-equilibrium using exciton model and direct reaction using the optical model parameters given in RIPL-3 library. The present version of the EMPIRE code is the latest version. EMPIRE makes use of several codes, written by different authors, which were converted into subroutines and adapted for the present use [17]. For the present work, the level density parameter was changed to get the best agreement with the measured data

(Level density parameter for EGSM, Gilbert-Cameron (EMPIRE) and GSM (RIPL) models [18,19].

Both the codes were used to calculate cross section for the selected reactions and are plotted in the Figs.2-7 along with the previous data. There is a fairly good agreement between present measurements with those of calculated results using TALYS-1.6 and EMPIRE-3.2.2. The present experimental result and theoretical predictions using above codes are also listed in Table-2.

IV. CONCLUSIONS

In the present study the (n,p) reaction cross section for some of the structural materials such as ^{75}As , ^{66}Zn , ^{64}Zn , ^{55}Mn , ^{51}V and ^{58}Ni were studied at 14.2 ± 0.2 MeV. The present results were compared with the previously measured data available in EXFOR database as well as theoretical predictions using code TALYS-1.6 and EMPIRE-3.2. Present results are in fairly good agreement with some previous measurements and also with theoretical predictions.

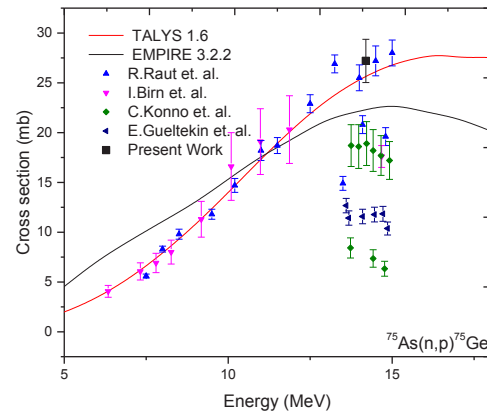


Fig. 2. Comparison of measured $^{75}\text{As}(n,p)^{75}\text{Ge}$ cross section with EMPIRE-3.2.2, TALYS-1.6, EXFOR

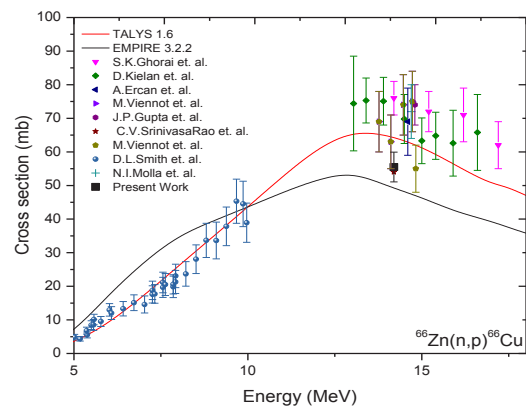


Fig. 3. Comparison of measured $^{66}\text{Zn}(n,p)^{66}\text{Cu}$ cross section with EMPIRE-3.2.2, TALYS-1.6, EXFOR

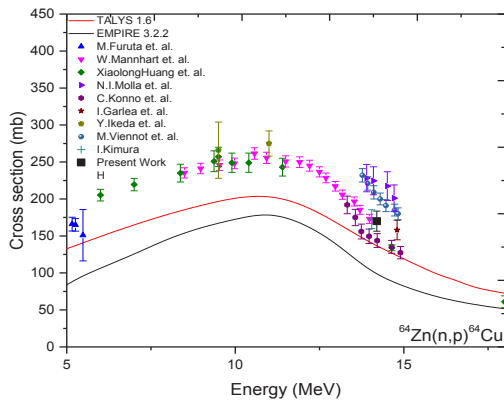


Fig. 4. Comparison of measured $^{64}\text{Zn}(n,p)^{64}\text{Cu}$ cross section with EMPIRE-3.2.2, TALYS-1.6, EXFOR

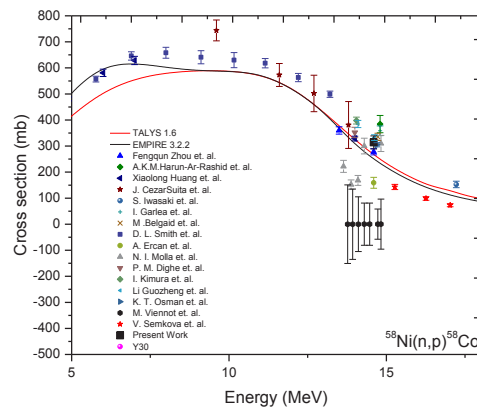


Fig. 7. Comparison of measured $^{58}\text{Ni}(n,p)^{58}\text{Co}$ cross section with EMPIRE-3.2.2, TALYS-1.6, EXFOR

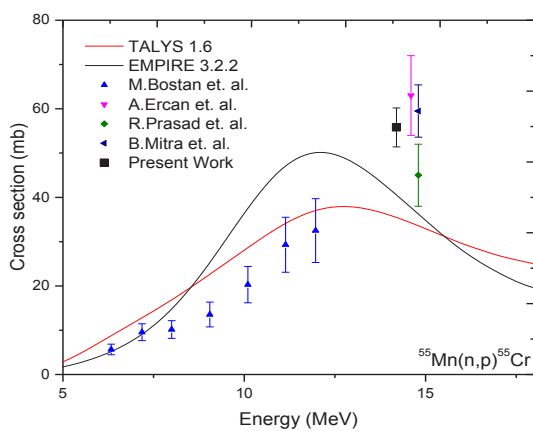


Fig. 5. Comparison of measured $^{55}\text{Mn}(n,p)^{55}\text{Cr}$ cross section with EMPIRE-3.2.2, TALYS-1.6, EXFOR

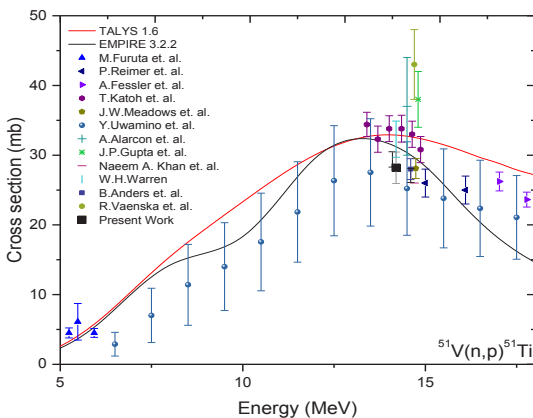


Fig. 6. Comparison of measured $^{51}\text{V}(n,p)^{51}\text{Ti}$ cross section with EMPIRE-3.2.2, TALYS-1.6, EXFOR

ACKNOWLEDGMENT

The authors thank to (Late) Prof. J. Rama Rao and (Late) Prof. L. Chaturvedi for their support to carry out neutron activation measurements at BHU, Varanasi, India.

REFERENCES

- [1] N.L. Singh, et al., Proc. of DAE Sympo. on Nucl. Phys. 59 (2014) 566. ; 60 (2015) 442.
- [2] N.L. Singh, P.M. Prajapati, Proc. of Electric Power Engineering, EPE-2014, 739-742 (2014).
- [3] International Atomic Energy Agency – Nuclear Data Section (team of authors), “Experimental Nuclear Reaction Data Library (EXFOR)”; <https://www-nds.iaea.org/exfor>, cited March 10, 2016.
- [4] A.R. Farhan, S. Rab, “Nuclear Datasheet for A=75”, Nucl. Dat. Sheets 60, 735 (1990).
- [5] M.R. Bhat, “Nuclear Datasheet for A=75”, Nucl. Dat. Sheets 83, 789 (1998).
- [6] Huo Junde, “Nuclear Datasheet for A=75”, Nucl. Dat. Sheets 64, 723 (1991).
- [7] B. Singh, “Nuclear Datasheet for A=75”, Nucl. Dat. Sheets 78, 395 (1996).
- [8] R.L. Auble, “Nuclear data sheets for A = 51”, Nucl. Dat. Sheets 23, 163 (1978).
- [9] C.D. Nesaraja, S.D. Geraedts, B. Singh, “Nuclear Datasheet for A=58”, Nucl. Dat. Sheets 111, 897 (2010).
- [10] A.J.Koning, et. al., “TALYS-1.6, A Nuclear reaction program”, user’s manual, NRG-1755 ZG Petten, The Netherlands (2011).
- [11] M. Herman, et. al., “EMPIRE-3.2.2 modular system for nuclear reaction calculations and nuclear data evaluation”, user’s manual, 2013.
- [12] J. Raynal, “Notes on ECIS94”, CEA Saclay Report No. CEA-N-2772, (1994).
- [13] A.J.Koning and J.P. Declaroche, Nucl.Phys., A713, 231-310(2003).
- [14] W. Hauser and H. Feshbach, Phys. Rev, 87, 366(1952).
- [15] C. Kalbach, Phy.Rev.C 33, 818–833 (1986).
- [16] S. Hofmann, et al., Ann. Phys. 90, 403 (1975); S. Hofmann, et al., Z. Physik A 297,153 (1980).
- [17] A.V. Ignatyuk, J. Nucl Phys. 21, 255 (1975).
- [18] A. Gilbert, et al., Can J. Phys. 43, 1446 (1965).
- [19] S. Hilaire, et al., Nucl. Phys, A779: 63-81(2006).

Measurements of the cross sections of $^{186}\text{W}(n, \gamma)^{187}\text{W}$, $^{182}\text{W}(n, p)^{182}\text{Ta}$, $^{154}\text{Gd}(n, 2n)^{153}\text{Gd}$, $^{160}\text{Gd}(n, 2n)^{159}\text{Gd}$ reactions at neutron energies between 5 to 17 MeV

Rajnikant Makwana¹, S. Mukherjee^{1,*}, P. Mishra¹, H. Naik², N. L. Singh¹, M. Mehta³,
K. Katovsky⁴, S. V. Suryanarayana⁵, V. Vansola¹, Y. Santhi Sheela⁶, M. Karkera⁶,
R. Acharya², S. Khirwadkar³

¹Physics Department, Faculty of Science, The Maharaja Sayajirao University of
Baroda, Vadodara-390002, India

²Radiochemistry Division, Bhabha Atomic Research Centre, Mumbai – 400 085,
India

³Divertor Division, Institute for Plasma Research, Gandhinagar – 382 428,
India

⁴Brno University of Technology, Department of Electrical Power Engineering, Brno,
Česká Republika

⁵Nuclear Physics Division, Bhabha Atomic Research Centre, Mumbai - 400 085,
India

⁶Manipal University, Department of Statistics, Manipal-576 104, India

The cross sections of the $^{186}\text{W}(n, \gamma)^{187}\text{W}$, $^{183}\text{W}(n, p)^{183}\text{Ta}$ and $^{154}\text{Gd}(n, 2n)^{153}\text{Gd}$, $^{160}\text{Gd}(n, 2n)^{159}\text{Gd}$ reactions were measured at the neutron energies 5.08 ± 0.165 , 8.96 ± 0.77 , 12.47 ± 0.825 and 16.63 ± 0.95 MeV. Standard neutron activation analysis technique and off-line gamma ray spectrometry were used for the measurement and analysis of the data. Measurements are done in the energy range, where few or no measured data are available. The results from the present work are compared with the literature data based on the EXFOR compilation. The experimental results are supported by theoretical predictions using nuclear modular codes TALYS – 1.8 and EMPIRE – 3.2.2. The predictability of different models available in TALYS – 1.8 and level models in EMPIRE – 3.2.2 were tested. A detailed comparison of experimental results with theoretical model calculations is made.

(*) Corresponding Author: sk.mukherjee-phy@msubaroda.ac.in

I. INTRODUCTION

Nuclear reaction cross section data is of prime importance for reactor technology. When the reactor is in operation, it produces neutrons that penetrate through several materials, such as fuel, structural, controlling and shielding materials, etc. It is important to have nuclear reaction cross section data for all these materials, at all possible neutron energies [1] for the development of the reactor technology. There are numerous measured nuclear data available in the EXchange FORmat (EXFOR) library [2]. However, it is important to have more experimental nuclear data, measured with high accuracy in the energy range between thermal to 20 MeV for a number of reactor materials [2]. Tungsten (W) and gadolinium (Gd) are two such materials. W is selected as a diverter material for the upcoming fusion device – International Thermonuclear Experimental Reactor (ITER) [3]. In ITER the DT reaction generates 14.6 MeV neutrons, which are scattered from the surrounding materials, thus neutrons will have energies from thermal to 14.6 MeV [4-9]. These neutrons interact with the diverter material of the reactor and can open different nuclear reaction channels. In Accelerator Driven Subcritical system (ADSs), W is used in different parts, hence it can face neutrons with higher energies [10]. Further, Gd is an important rare earth element, which is used in control rods. Its nitrate form is useful for reactor control through moderator as liquid poison, as well as a secondary shutdown device in PHWR reactors [11]. Gadolinium nitrate is more advantageous due to its properties, such as; high thermal neutron capture cross section, quick burnout, greater solubility and a more efficient removal by ion exchange systems compared with boron [12]. Hence it is important to have accurate cross section data for all the tungsten and gadolinium isotopes in the energy range from thermal to 20 MeV. Accurate experimental data is also needed to validate the various theoretical nuclear models [13]. In view of this, in the present work, cross sections for the $^{186}\text{W}(n, \gamma)^{187}\text{W}$, $^{183}\text{W}(n, p)^{183}\text{Ta}$, $^{154}\text{Gd}(n, 2n)^{153}\text{Gd}$ and $^{160}\text{Gd}(n, 2n)^{159}\text{Gd}$ reactions at the neutron energies of 5.08 ± 0.165 , 8.96 ± 0.77 , 12.47 ± 0.825 and 16.63 ± 0.95 MeV were measured by neutron activation analysis (NAA) and the off-line gamma ray spectrometry technique. The above mentioned reaction cross-sections were also calculated by using the computer codes TALYS – 1.8 and EMPIRE – 3.2.2. Different ldmodels available in TALYS – 1.8 and

levden models in EMPIRE – 3.2.2 were used to validate the present experimental results.

In this paper, the experimental details are discussed in section II. Section III describes the data analysis. The neutron flux and average neutron energy calculations used to obtain reaction cross sections, with suitable corrections incorporated to obtain accurate cross section results, are also discussed in this section. Section IV presents the theoretical calculations, followed by results and discussions in section V. A summary and conclusions are given in section VI.

II. EXPERIMENTAL DETAILS

The experiment was carried out by using the BARC-TIFR Pelletron facility in Mumbai, India. The neutrons were produced using the ${}^7\text{Li}(p, n){}^7\text{Be}$ reaction. A proton beam was targeted on natural lithium foil of thickness 8.0 mg/cm^2 . The Li foil was wrapped with 3.7 mg/cm^2 tantalum in front and 4.12 mg/cm^2 on the back. The energies of the proton beam were selected to be 7.0, 11.0, 15.0 and 18.8 MeV. The samples were kept at a distance of 2.1 cm from the Li – target in the forward direction. The targets were irradiated for different irradiation times. The irradiation details are given in [Table I](#). A schematic view of the irradiation setup is shown in [Fig. 1](#). In the present measurements, the natural samples of W (99.97 %) in the form of 1.0 mm thick and about a quarter of a circle with radius of 1 to 3 cm were used. Gd samples were made in the form of a pellet with radius of 0.65 cm and of thickness from 0.5 to 1.0 mm using Gd_2O_3 (99.9 %) powder. The weight of the samples was measured using digital micro balance weighing machine. The mass of W samples in different sets of irradiations were 3.6689 g (Irradiation – 1), 0.7826 g (Irradiation – 2), 0.8344 g (Irradiation – 3) and 0.504 g (Irradiation – 4). The samples of Gd were with mass of 0.4071 g (Irradiation – 1) and 0.9102 g (Irradiation – 3). In each irradiation, indium (In) and thorium (Th) foils were used as flux monitors. After a suitable cooling time, the irradiated samples were mounted on different Perspex plates and kept in front of the pre-calibrated High Purity Germanium (HPGe) detector. A Baltic company HPGe detector with 4k channels MCA and MAESTRO spectroscopic software was used to measure the gamma ray spectra from the irradiated sample. The HPGe detector system was calibrated using a standard ${}^{152}\text{Eu}$ multi-gamma ray source. The efficiency of the detector was also determined at different gamma energies using the same source. The gamma ray activities of the irradiated samples were measured for different counting times. The prominent gamma ray energies emitted from the irradiated samples and other spectroscopic data are given

in Table II. Isotopic abundances are taken from the literature [14]. The threshold energies of the reactions are calculated using the Q – value calculator provided online by NNDC [15]. The daughter nuclide half-life and details of the emitted prominent gamma rays are taken from literature [16]. Typical gamma ray spectra obtained from the irradiated W and Gd samples are shown in Figs. 2 (a-b).

Table I. Details of the irradiation in the present experiment

	Irradiation - 1	Irradiation - 2	Irradiation - 3	Irradiation - 4
Proton Energy (MeV)	18.8	7.0	15.0	11.0
Total Irradiation Time (hr:min)	5:00	11:15	7:00	16:05
Beam Current (nA)	150	110	150	120

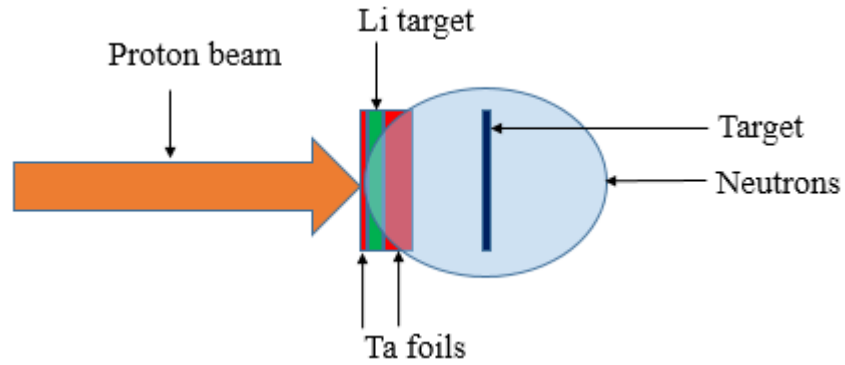


FIG. 1. (Color online) Experimental arrangement showing neutron production using Li(p, n) reaction

Table II. Selected nuclear reactions, target isotopic abundance, threshold energy of reaction, product nucleus with half-life and energies of prominent gamma rays with branching intensities.

Reaction	Isotopic Abundance (%) [14]	Threshold Energy (MeV) [15]	Product Nucleus	Half-life [16]	Prominent γ -ray Energy (keV); (Branching intensity %)
$^{186}\text{W}(n, \gamma)^{187}\text{W}$	28.43	-	^{187}W	24.0 h	479.5(26.6); 685.7(33.2)
$^{182}\text{W}(n, p)^{182}\text{Ta}$	26.50	1.037	^{182}Ta	114.74 d	1121.3(35.24)
$^{154}\text{Gd}(n, 2n)^{153}\text{Gd}$	2.18	8.953	^{153}Gd	240.4 d	103.1 (21.1)
$^{160}\text{Gd}(n, 2n)^{159}\text{Gd}$	21.86	7.498	^{159}Gd	18.479 h	363.5 (11.78)

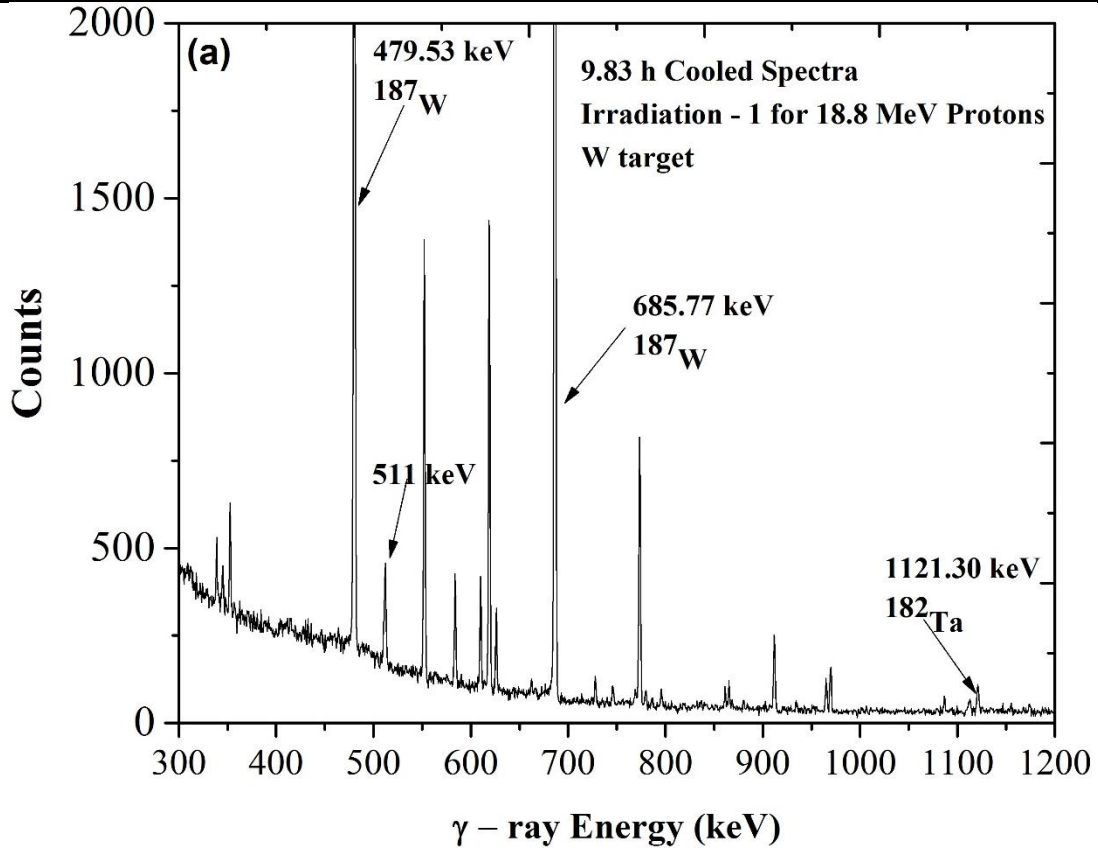


FIG. 2 (a). Typical γ -ray spectra for W target obtained by using HPGe detector

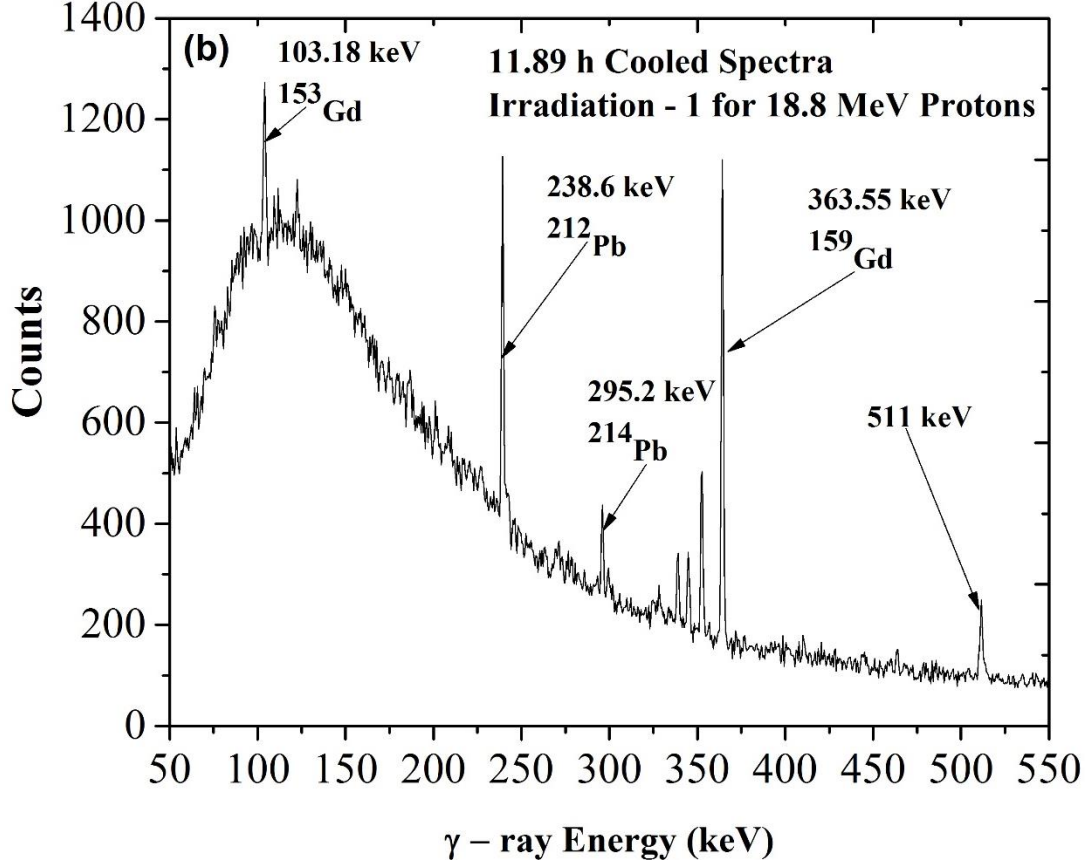


FIG. 2 (b). Typical γ -ray spectra for Gd target obtained by using HPGe detector

III. DATA ANALYSIS

A. Neutron Activation Analysis

The experimental data were analyzed by using the standard neutron activation analysis (NAA) technique. In this technique, the nuclear reaction rate or the rate of production of daughter isotopes depends on the number of target nuclei available and the neutron flux incident on it. This activation method is generally followed to measure reaction cross section by irradiating the target isotope with neutrons, when the products emit characteristic gamma rays having sufficiently long half-life and gamma branching abundances. The cross section of the selected reactions can be determined using the following equation [17].

$$\sigma = \frac{A_{\gamma} \cdot \lambda \cdot (t_c / t_r)}{N \cdot \phi \cdot I_{\gamma} \cdot \varepsilon \cdot (1 - e^{-\lambda \cdot t_i}) \cdot (1 - e^{-\lambda \cdot t_c}) \cdot e^{-\lambda \cdot t_w}} \quad (1)$$

Where,

A_{γ} = Number of detected gamma ray counts;

λ = Decay constant of product nucleus (s^{-1})

- t_i = Irradiation time (s);
 t_w = Cooling time (s);
 t_c = Counting time (s);
 t_r = Real time (Clock time) (s);
 ϕ = Incident neutron flux ($n\text{ cm}^{-2}\text{s}^{-1}$);
 I_γ = Branching intensity of γ -ray;
 ε = Efficiency of detector for the chosen gamma ray;
 N = Number of target atoms

In the above equation, the activity (A_γ) is measured using an HPGe detector for different gamma rays emitted from the daughter isotopes. Because of the half-lives of the isotopes of interest, several rounds of gamma ray counting were done. The dead time of the detector system was kept below 0.6 % during the entire counting process. The numbers of target nuclei were calculated from the weight of the sample and isotopic abundances. The calculation of the neutron flux was done using the gamma ray spectra of irradiated In and Th foils. Other standard parameters of the reactions were taken from the literature [14-16].

B. Neutron flux and Average neutron energy

The neutrons were generated by ${}^7\text{Li}(p, n){}^7\text{Be}$ reactions. Below 2.4 MeV, this reaction produces mono-energetic neutrons [18]. Above 2.4 MeV, the first excited state of ${}^7\text{Be}$ at 0.43 MeV is populated and produces a second group of neutrons [18, 19]. Above 6 MeV, the three body interaction, and other excited states also contribute in the neutron production along with the main neutron group [18, 19]. Although there are lower energy sub-group of neutrons, the primary (main) group of neutrons can be used to measure the reaction cross section as it has higher neutron flux and higher neutron energy (forming a peak). The reaction cross section measured at this averaged peak energy. The spectrum averaged neutron energy can be given as [20],

$$E_{mean} = \frac{\int_{E_{ps}}^{E_{max}} E_i \phi_i dE}{\int_{E_{ps}}^{E_{max}} \phi_i dE} \quad (2)$$

Where,

E_{ps} = peak forming start neutron energy

E_{max} = maximum neutron energy

E_i = energy bin

ϕ_i = neutron flux of energy bin E_i

E_{mean} = effective mean energy

The neutron spectra for 7.0, 11.0, 15.0 and 18.8 MeV were derived by taking data from various available publications [18-22]. The neutron spectra corresponding to all the four incident proton energies are shown in Fig. 3 (a – d). The average peak energies obtained by using equation (2) are given in Table III.

In order to analyze the data, it is necessary to accurately calculate the neutron flux incident on the target. In the present experiment, $^{115}\text{In}(n, n')^{115\text{m}}\text{In}$ and $^{232}\text{Th}(n, f)^{97}\text{Zr}$ monitor reactions were used for the neutron flux measurement. The reaction products $^{115\text{m}}\text{In}$ and ^{97}Zr have a half-life of 4.486 h and 16.749 h respectively [16]. The emitted characteristic gamma lines are given in Table IV. Typical gamma ray spectra obtained from both the monitors are shown in Fig. 5.

The calculations of the neutron flux incident on the target were done by using the spectrum averaged neutron cross section for the monitor reactions by using the relatively recent data available from the EXFOR data library for $^{115}\text{In}(n, n')$ [23- 26] and for $^{232}\text{Th}(n, f)$ [27-30]. The spectrum averaged cross section was calculated using the following equation,

$$\sigma_{av} = \frac{\int_{E_{th}}^{E_{max}} \sigma_i \phi_i dE}{\int_{E_{th}}^{E_{max}} \phi_i dE} \quad (3)$$

Where,

E_{th} = threshold energy of the monitor reaction

E_{max} = maximum neutron energy

σ_i = Cross section at energy E_i for monitor reaction from EXFOR [23-30]

ϕ_i = neutron flux of energy bin E_i from the Fig. 4 (a – d)

σ_{av} = Spectrum averaged cross section

The calculated spectrum averaged cross sections for both the monitor reactions are given in Table III. The neutron flux incident on targets for all the four irradiations were calculated using the following activation equation (1).

$$\phi = \frac{A_\gamma \cdot \lambda \cdot (t_c / t_r)}{N \cdot \sigma_{av} \cdot I_\gamma \cdot \varepsilon \cdot (1 - e^{-\lambda \cdot t_i}) \cdot (1 - e^{-\lambda \cdot t_c}) \cdot e^{-\lambda \cdot t_w}} \quad (4)$$

All the parameters are same as in equation (1).

In the case of fission reaction monitor, the fission yield term (Y) will come in the denominator on the right side of the above equation (4). In the cross section calculations, the measured values of the average neutron flux from both the monitors were taken, as both these values are in agreement with each other within the limits of the experimental errors as discussed later in section V.

C. Cross section correction for lower energy neutrons

In order to measure the cross section for neutrons of main peak, it is necessary to make corrections due to the contributions from lower energy neutrons. This correction is not required when the neutron source is purely mono-energetic, which is not the present case. As mentioned earlier, in addition to a primary neutron group, there exist secondary neutron groups arising due to an excited state of ^7Be and three-body reactions above 2.4 and 6 MeV respectively [18]. These secondary groups produce neutrons, at lower energies and in addition to the primary group neutrons [18, 19]. As the primary neutron exhibit a distinct broad peak always at much higher energy with a high neutron flux, it can be considered as quasi mono-energetic source. It is possible to remove the contributions to the reaction cross sections due to low energy neutrons from the primary neutron group by the process of making a tailing correction. In the present work, the tailing correction has been done using the method given in the literature [20].

The cross sections have been calculated using the NAA equation (1) and the neutron flux from monitor reactions. For a capture reaction, one has to use total neutron flux, but for the reactions having threshold energy, the neutron flux must be corrected. To do this, one has to remove the neutron flux from minimum to threshold energy neutrons, by taking the area under the neutron spectra. For instance, the $^{154}\text{Gd}(n, 2n)^{153}\text{Gd}$ reaction has a threshold energy of 8.953 MeV. Hence, the flux for this reaction must be the area under the curve shown from 'A' (threshold energy) to 'B' (maximum neutron energy) [Fig 4]. This will correct the actual neutron flux used to produce the desired daughter isotopes. Using this neutron flux, a set of cross sections of all reactions has been calculated. In order to remove the effective spectrum average cross section from the threshold to the minimum energy of the peak of interest (E_{ps}), theoretical calculations using modular code TALYS – 1.8 have been carried out to obtain the reaction cross sections versus neutron energy. These calculated cross sections at different energies are convoluted with the neutron flux as shown in Fig. 3 (a). The

spectrum average cross section for each reaction was calculated from threshold to minimum energy (E_{ps}), and it is subtracted from the previous cross section dataset. Thus the final value obtained gives the cross section for the reaction at the spectrum average neutron peak energy.

Using the above method, the cross sections for the $^{182}\text{W}(n, p)^{182}\text{Ta}$, $^{186}\text{W}(n, \gamma)^{187}\text{W}$, $^{154}\text{Gd}(n, 2n)^{153}\text{Gd}$ and $^{160}\text{Gd}(n, 2n)^{159}\text{Gd}$ reactions were measured at the neutron energies of 5.08, 8.96, 12.47 and 16.63 MeV. In the $^{160}\text{Gd}(n, 2n)^{159}\text{Gd}$ and $^{158}\text{Gd}(n, \gamma)^{159}\text{Gd}$ reactions, a common γ -ray of 363.54 keV ($I_\gamma = 11.78\%$) is emitted. Therefore, it is necessary to remove this part of the cross section from this capture reaction. At higher energies, the (n, γ) reaction has a very small contribution compared to the lower energy neutrons. Since the lower energy neutron part has been already corrected using above method, therefore the cross section obtained is purely due to the $(n, 2n)$ reaction. In the same way, the tailing corrections have been applied for all the reactions studied in the present work.

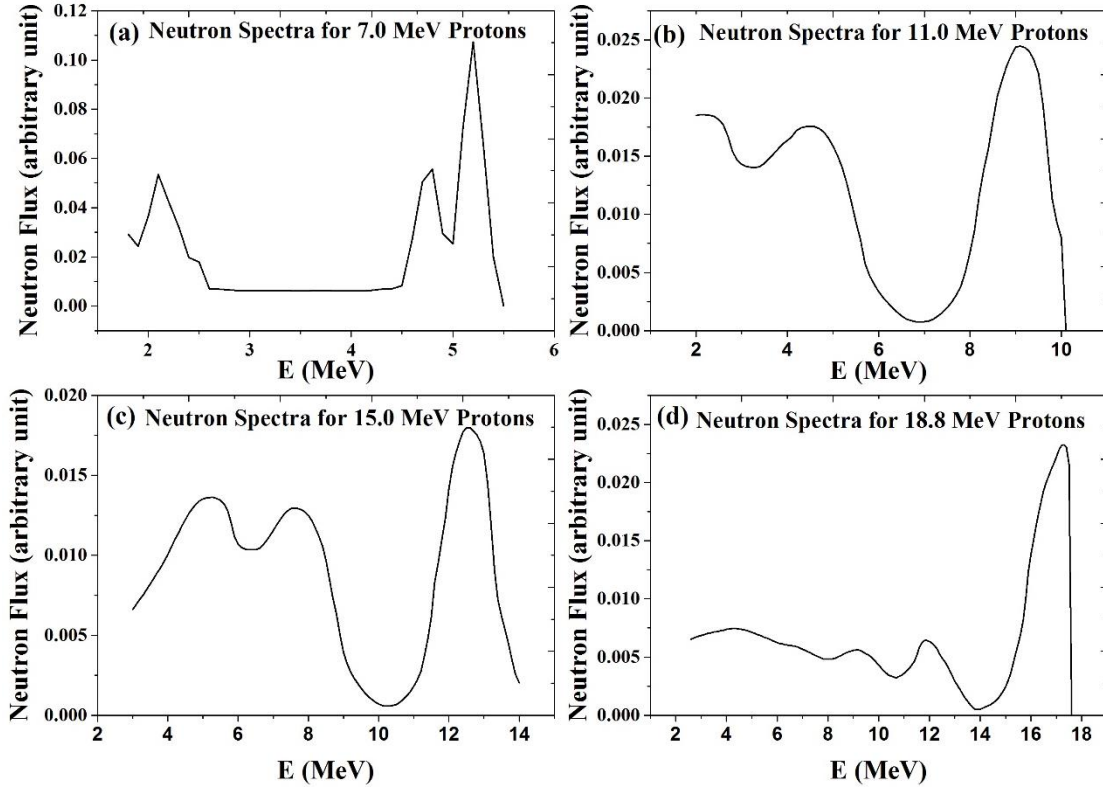


FIG. 3 (a – d). $^7\text{Li}(p, n)^7\text{Be}$ neutron spectra for the 7.0 (a), 11.0 (b), 15.0 (c) and 18.8 (d) MeV proton energies

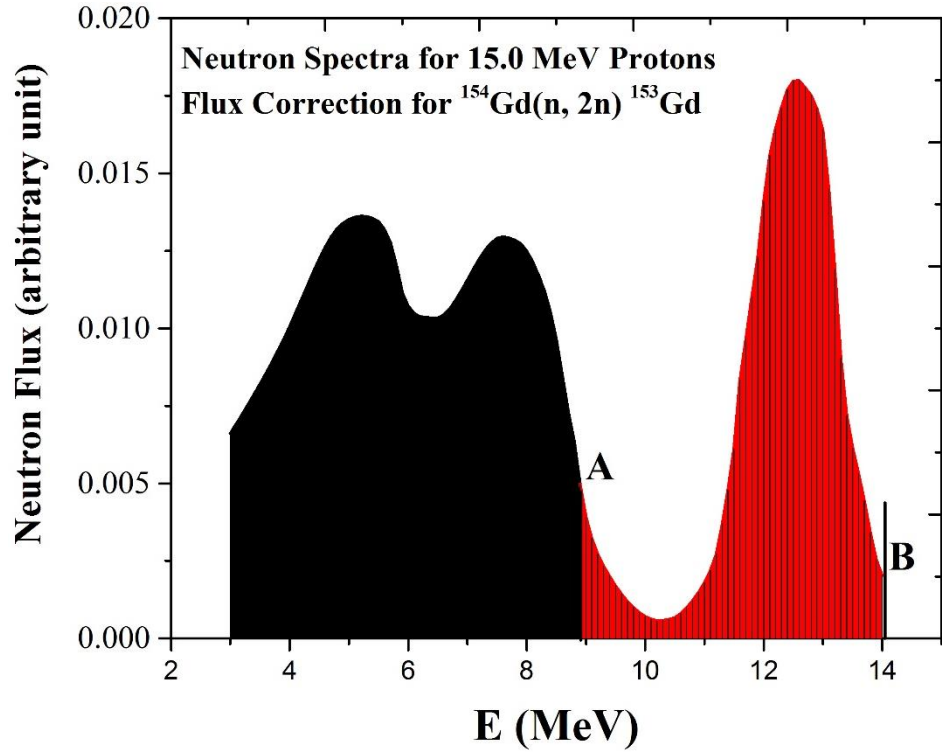


FIG. 4. (Color online) Neutron flux correction for the threshold energy reactions, shown for $^{154}\text{Gd}(n, 2n)^{153}\text{Gd}$ reaction with threshold energy of 8.953 MeV labeled by 'A' and maximum neutron energy labeled by 'B'

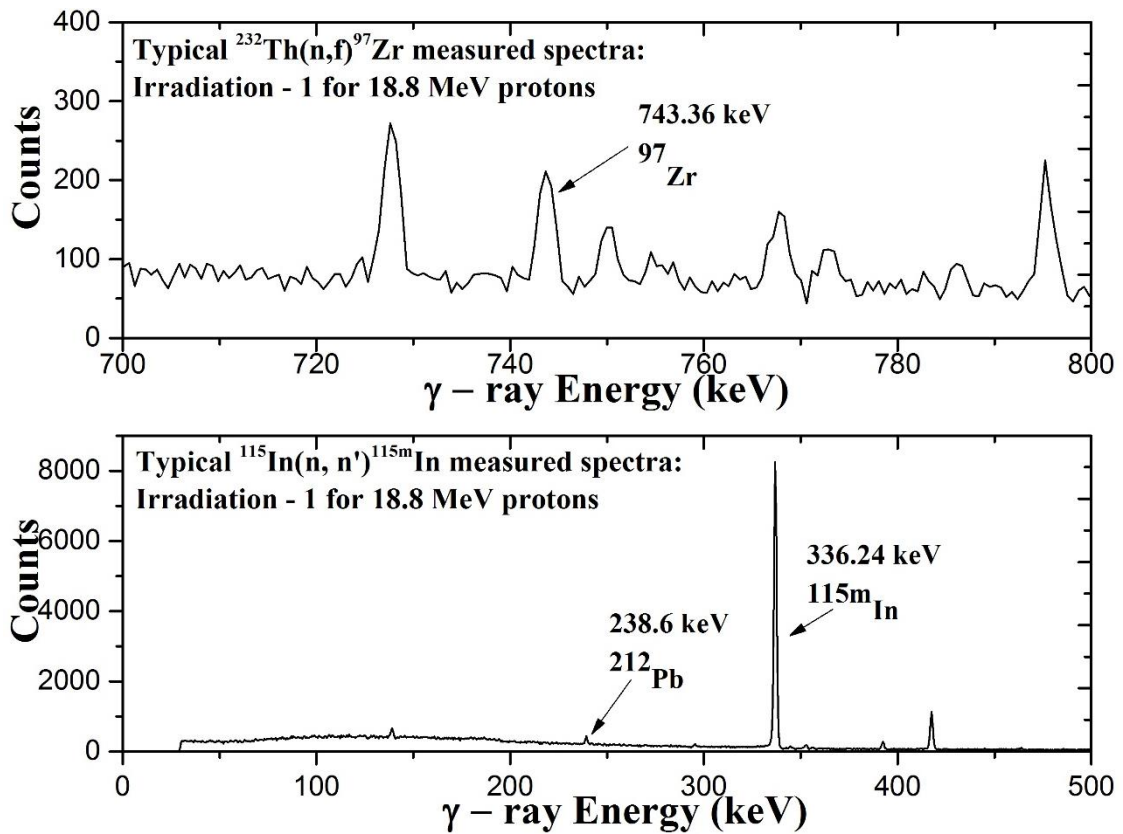


FIG. 5. Typical monitor reaction gamma ray spectra using HPGe detector

Table III. The spectrum averaged neutron energies and respective neutron flux from two different monitor reactions

	Irradiation - 1	Irradiation-2	Irradiation-3	Irradiation-4
Proton Energy (MeV)	18.8	7.0	15.0	11.0
Neutron Energy from eq. (2) (MeV)	16.63 ± 0.95	5.08 ± 0.165	12.47 ± 0.825	8.96 ± 0.77
Spectrum Averaged Cross section for In monitor (mb)	188.94	223.88	253.79	302.85
Calculated Neutron Flux from $^{115}\text{In}(n, n')^{115\text{m}}\text{In}$ ($\text{n cm}^{-2} \text{s}^{-1}$)	6.2891×10^7	4.6304×10^6	1.8054×10^7	1.6009×10^6
Spectrum Averaged Cross section for Th monitor (mb)	341.67	99.04	269.58	220.01
Calculated Neutron Flux from $^{232}\text{Th}(n, f)^{97}\text{Zr}$ ($\text{n cm}^{-2} \text{s}^{-1}$)	6.2885×10^7	4.5709×10^6	1.7090×10^7	1.5850×10^6

Table IV. The monitor reaction with the product nucleus and prominent gamma lines

Monitor Reaction	Product Nucleus (Half-life) [16]	Prominent gamma Line (branching Intensity %) [16]
$^{115}\text{In}(n, n')^{115\text{m}}\text{In}$	$^{115\text{m}}\text{In}$ (4.486 h)	336.24 (45.8)
$^{232}\text{Th}(n, f)^{97}\text{Zr}$	^{97}Zr (16.749 h)	743.36 (93.0)

IV. THEORETICAL CALCULATIONS

In order to theoretically understand the measured cross section results, two well-known nuclear reactions modular codes TALYS – 1.8 and EMPIRE – 3.2.2 were used [13]. Both the codes are being used worldwide for nuclear data prediction for the emission of gamma, neutron, proton, deuteron, triton and other particles. Both codes used the reaction parameters from the RIPL database [31]. These codes consider the effect of level density parameters, compound, pre-equilibrium and direct reaction mechanism as a function of incident particle energy. The optical model parameters were obtained by using a global potential, proposed by Koning and Delaroche [32]. The compound reaction mechanism was incorporated using the Hauser-Feshbach model [33]. The pre-equilibrium contribution was accounted for by an exciton model that was developed by Kalbach [34]. In the present work, the calculations have been done with all the default parameters except changing the *ldmodel* and level density parameters. The present results along with EXFOR data were compared with these predicted data as shown in Figs. 6 (a-b).

V. RESULTS & DISCUSSION

The main objective of the present study was to provide a set of reaction cross section data in the energy range where there are very few or no measurements available in the literature. These cross sections are important for the accurate reactor design and also to improve the existing nuclear database. Hence the present experimental data for W and Gd isotopes become more important. Further, in this energy region, the standard nuclear models play an important role to validate the present measured experimental data. The major uncertainties in the present reaction cross sections are given in Table V.

The measured data were supported by the theoretical predictions using EMPIRE – 3.2.2 and TALYS – 1.8. There are different options of level density given in EMPIRE – 3.2.2. The level density parameter values *levden* = 0, 1, 2, 3, 4 uses various well known models described in various publications [31, 35-39]. By varying these parameters, the cross section for the selected reactions from threshold to 20 MeV were calculated. The predicted and experimental results are shown in Figs. 6 (a-d). In TALYS – 1.8, the different *ldmodel* options were varied from *ldmodel1* to *ldmodel6* for the selected nuclear reactions and the experimental cross sections were compared. The details of these parameters are given in the TALYS – 1.8 manual [39, 40].

As shown in Fig. 6 (a) for $^{186}\text{W}(n, \gamma)^{187}\text{W}$ reaction, the *levden* = 2 of EMPIRE – 3.2.2 gives a relatively better agreement compared to other *levden* values. But at lower

energy the levden = 2 does not give satisfactory predictions. Moreover, all other level density models of EMPIRE – 3.2.2 show discrepancies with each other and predicts lower cross section as compared to the present experimental results. In the case of TALYS – 1.8 analyses, results of all the ldmmodels options are in good agreement with the data of present measurements. For the $^{182}\text{W} (n, p) ^{182}\text{Ta}$ reaction, all TALYS – 1.8 ldmmodels are in good agreement. The EMPIRE levden models show a discrepancy with most of EXFOR and the present data. For the $^{154}\text{Gd} (n, 2n) ^{153}\text{Gd}$ and $^{160}\text{Gd} (n, 2n) ^{159}\text{Gd}$ reactions, the experimental results are in good agreement with both the TALYS – 1.8 and EMPIRE – 3.2.2 predictions, except levden = 2, being listed as a future option in the EMPIRE input file. Only the measurement at 16.63 MeV neutron energy of $^{160}\text{Gd}(n, 2n)^{159}\text{Gd}$ is under estimated then the predicted values. Overall the theoretical predictions support the present results. The measured cross section values and the different model predicted values are compared at the same energies in [Table VI](#). In general, TALYS – 1.8, for all the selected models, gives better agreement compared to EMPIRE – 3.2.2 in predicting the present experimental results.

Table V. Major uncertainties incorporated in the present cross section results

Parameter	Limit (%)
Counting rate	$\leq 4 - 5$
Efficiency Calibration	≤ 3
Self - absorption	≤ 0.2
Mass	≤ 0.001
Neutron flux	≤ 6
I_γ	≤ 3

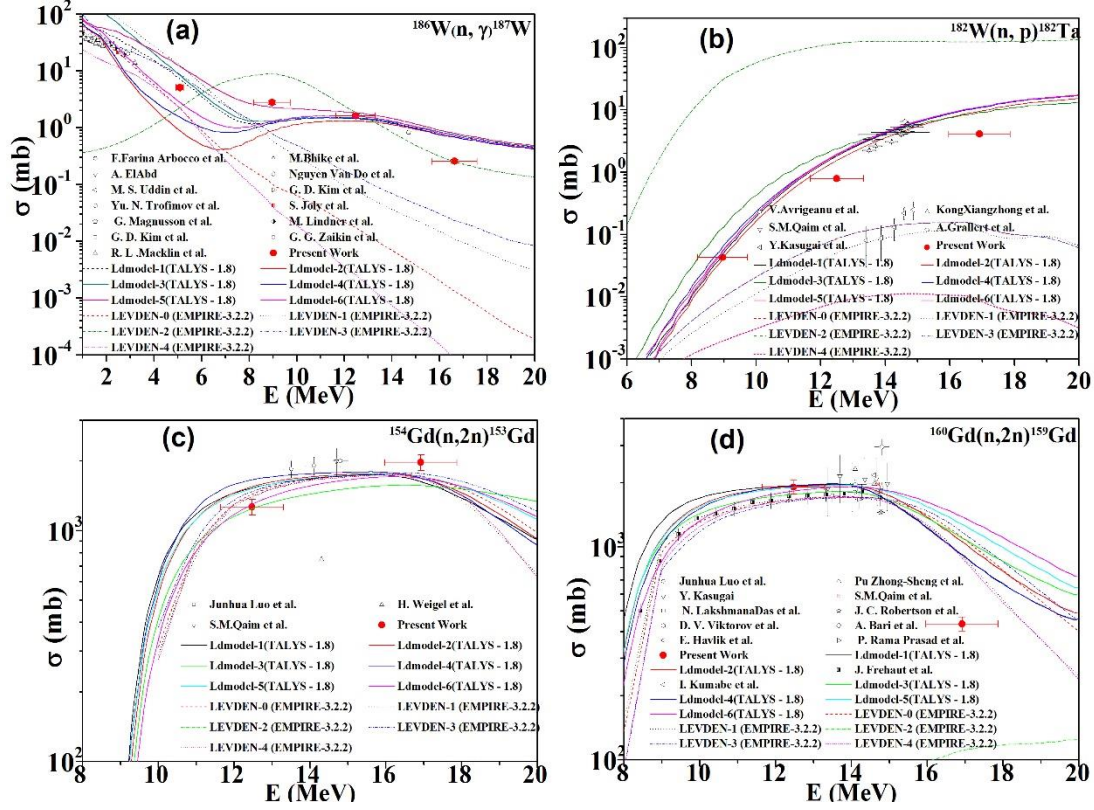


FIG. 6 (a – d). (Color online) Present measured cross section for $^{186}\text{W}(n, \gamma)^{187}\text{W}$ and $^{182}\text{W}(n, p)^{182}\text{Ta}$, $^{154}\text{Gd}(n, 2n)^{153}\text{Gd}$ and $^{160}\text{Gd}(n, 2n)^{159}\text{Gd}$ reactions compared with EXFOR and predicted cross section data using different theoretical nuclear models of TALYS – 1.8 and EMPIRE – 3.2.2; The LEVDEN-2 model of EMPIRE – 3.2.2 predicts very low values (below 100 mb) of cross sections comparing to other models hence it cannot be seen in plot of $^{154}\text{Gd}(n, 2n)^{153}\text{Gd}$

VI. SUMMARY & CONCLUSIONS

Cross section for the $^{182}\text{W}(n, p)^{182}\text{Ta}$, $^{186}\text{W}(n, \gamma)^{187}\text{W}$, $^{154}\text{Gd}(n, 2n)^{153}\text{Gd}$ and $^{160}\text{Gd}(n, 2n)^{159}\text{Gd}$ reactions were measured at the neutron energies 5.08 ± 0.165 , 8.96 ± 0.77 , 12.47 ± 0.825 and 16.63 ± 0.95 MeV by using the neutron activation analysis technique and incorporating standard tailing corrections [18]. The cross sections have been measured in an energy range where very few or no measurements are available. The different correction terms are discussed in order to achieve accurate cross section results. The spectrum averaged neutron energy and accurate flux measurements have also been duly incorporated. The neutron flux at different energies have been calculated by using two monitor reactions and the values thus obtained were found to be in good agreement. The average flux values from the two monitor reactions were taken for cross sections calculation. The cross section for the $^{186}\text{W}(n, \gamma)^{187}\text{W}$ reaction have been measured at four different energies. In the case of $^{182}\text{W}(n, p)^{182}\text{Ta}$ the cross sections are

reported at 8.96 ± 0.77 , 12.47 ± 0.825 and 16.63 ± 0.95 MeV. For the $^{154}\text{Gd}(n, 2n)^{153}\text{Gd}$ and $^{160}\text{Gd}(n, 2n)^{59}\text{Gd}$ reactions, the cross sections are reported at 12.47 ± 0.825 and 16.63 ± 0.95 MeV neutron energies. All the measurements have been compared with the theoretical modular codes TALYS – 1.8 and EMPIRE – 3.2.2. It may be concluded that TALYS – 1.8 gives an overall satisfactory agreement with the present experimental and EXFOR results for most of the selected models as compared to EMPIRE – 3.2.2 predictions. However, in the case of (n,γ) reaction, levden = 2 of EMPIRE gives somewhat better predictions as compared to other levden models in the energy region above 12 MeV. The cross section data presented in this work are important for the future fission/fusion reactor technology.

Acknowledgements

One of the authors (SM) thanks the DAE-BRNS for the sanction of a major research project (Sanction Number: 36(6)/14/22/2016-BRNS). The authors are grateful to Dr. S. C. Sharma (Scientific Officer, BARC – TIFR Pelletron Accelerator Facility) for preparing Li-target and for his help in the experimental setup. The authors acknowledge gratefully the help of Prof. John F. Sharpey Schafer, Retired Professor, Liverpool University and former Director, iThemba LABS, South Africa, for his valuable suggestions and corrections in the manuscript. Thanks are also due to Nishant Barot, Naveen Agrawal, P. K. Mehta, and Ketan Chaudhari from the department for their help in the target preparation.

References

- [1] A. J. Koning, and J. Blomgren, Nuclear data for sustainable nuclear energy, JRC Scientific and Tech. Rep. EUR23977EN-2009, 15 (2009).
- [2] Cross Section Information Storage and Retrieval System (EXFOR), IAEA, Vienna, Austria. <http://www.nds.iaea.or.at/exfor/> (online).
- [3] M. Lehnen, *et al.*, J. Nucl. Mater. **463**, 39 (2013).

- [4] J. Qing, Y. Wu, M. Regis, and J. W. Kwan, IEEE Trans. Nucl. Sci. **56**, 1312 (2009).
- [5] J. Reijonen, F. Gicquel, S. K. Hahto, M. King, T. P. Lou, and K. N. Leung, Appl. Radiat. Isotopes **63**, 757 (2005).
- [6] Y. Wu, J. P. Hurley, Q. Ji, J. Kwan, and K. N. Leung, IEEE Trans. Nucl. Sci. **56**, 1306 (2009).
- [7] V. Voitsenya, *et al.*, Rev. Sci. Instrum. **72**, 475 (2001).
- [8] G. De Temmerman, R. A. Pitts, V. S. Voitsenya, L. Marot, G. Veres, M. Maurer, and P. Oelhafen, J. Nucl. Mater. **363**, 259 (2007).
- [9] K. H. Behringer, J. Nucl. Mater. **145**, 145 (1987).
- [10] Yousry Gohar, Igor Bolshinsky, and Ivan Karnaukhov, NEA/NSC/DOC (2015) 7, 254 (2015).
- [11] R. Vijayalakshmi, D. K. Singh, M. K. Kotekar, and H. Singh, J Radioanal. Nucl. Chem. **300**, 129 (2014)
- [12] S. Dutta, P. Suryanarayanan, A. R. Kandalgaonkar, R. S. Sharma, and H. Bose, BARC News Lett, **271**, 2 (2006).
- [13] N. Dzysiuk, I. Kadenko, A. J. Koning, and R. Yermolenko, Phys. Rev. C **81**, 014610 (2010).
- [14] K. J. R. Rosman, and P. D. P. Taylor, Pure Appl. Chem. **71**, 1593 (1999).
- [15] <http://www.nndc.bnl.gov/qcalc/index.jsp>, retrieved on 11th November 2016.
- [16] http://www.nndc.bnl.gov/nudat2/indx_dec.jsp, retrieved on 21st March 2017.
- [17] Vibha Vansola, *et al.*, Radiochim. Acta **103**, 817 (2015).
- [18] C. H. Poppe, J. D. Anderson, J. C. Davis, S. M. Grimes, and C. Wong, Phys. Rev. C **14**, 438 (1976).
- [19] J. D. Anderson, C. Wong, and V. A. Madsen, Phys. Rev. Letts. **24**, 1074 (1970).
- [20] D. L. Smith, *et al.*, “ Corrections for Low Energy Neutrons by Spectral Indexing”, Retrieved from: <https://www.oecdnea.org/science/docs/2005/nsc-wpec-doc2005-357.pdf>
- [21] P. M. Prajapati, *et al.*, Eur. Phys. J. A **48**, 1 (2012).
- [22] M. W. McNaughton, N. S. P. King, F. P. Brady, J. L. Romero, and T. S. Subramanian, Nucl. Instrum. Methods **130**, 555 (1975).
- [23] A. A. Lapenas, Neutron Spect. Meas. by Activ., Riga 1975, (1975).

- [24] G. Loevestam, M. Hult, A. Fessler, T. Gamboni, J. Gasparro, R. Jaime, P. Lindahl, S. Oberstedt, and H. Tagziria, Nucl. Instrum. Methods in Physics Res., Sect. A 580, 1400 (2007).
- [25] Y. Agus, I. Celenk, and A. Ozmen Radiochimica Acta 92, 63 (2004).
- [26] M. S. Uddin, Radiochimica Acta 101, 613 (2013).
- [27] O. A. Shcherbakov, *et al.*, Int. Sem. on Interactions of Neutrons with Nuclei 9, 257 (2001).
- [28] R. K. Jain, Pramana 49, 515 (1997).
- [29] I. Garlea, Chr. Miron-Garlea, and H. N. Rosu, Revue Roumaine de Physique 37, 19 (1992).
- [30] F. Manabe, K. Kanda, T. Iwasaki, H. Terayama, Y. Karino, M. Baba, and N. Hirakawa, Fac. of Engineering, Tohoku Univ. Tech. Report 52, 97 (1988).
- [31] R. Capote, *et al.*, Nuclear Data Sheets 110, 3107 (2009).
- [32] A. J. Koning, and J. P. Declaroche, Nucl. Phys. A 713, 231 (2003).
- [33] W. Hauser, and H. Feshbach, Phys. Rev. 87, 366 (1952).
- [34] C. Kalbach, Phys. Rev. C 33, 818 (1986).
- [35] <https://www-nds.iaea.org/RIPL-3/densities/>, retrieved on 28th February 2017.
- [36] A. V. Ignatyuk, K. K. Istekov, and G. N. Smirenkin, Sov. J. Nucl. Phys. 29, 450 (1979).
- [37] A. V. Ignatyuk, J. L. Weil, S. Raman, and S. Kahane, Phys. Rev. C 47, 1504 (1993).
- [38] A. Gilbert, and A. G. W. Cameron, Can. J. Phys. 43, 1446 (1965).
- [39] S. Hilaire, M. Girod, S. Goriely and A. J. Koning, Phys. Rev. C 86, 1 (2012).
- [40] A. Koning, S. Hilaire, and S. Goriely, TALYS-1.6 - A Nuclear Reaction Program, User Manual, 1st edition (NRG, The Netherlands, 2013).

Table VI. Comparison of present experimental data different model predictions using TALYS – 1.8 and EMPIRE – 3.2.2

Energy (MeV)	$^{186}\text{W}(n, \gamma)^{187}\text{W}$ reaction cross section (mb)																
	Measured				TALYS - 1.8								EMPIRE - 3.2.2				
5.08±0.165	5.079±0.39	Ldmodel-1	Ldmodel-2	Ldmodel-3	Ldmodel-4	Ldmodel-5	Ldmodel-6	Levden-0	Levden-1	Levden-2	Levden-3	Levden-4	8.83	2.2903	0.0453		
8.96±0.77	2.767±0.19	7.23	0.885	8.37	1.53	12.1	2.80	2.24	12.8	2.24	8.83	2.2903	0.827	0.0453			
12.47±0.825	1.620±0.11	1.22	0.871	1.31	1.17	2.26	1.26	0.108	0.618	9.01	0.827	0.0453	0.146	0.0027			
16.63±0.95	0.257±0.02	1.46	1.30	1.48	1.43	1.81	1.58	0.0181	0.0794	1.86	0.146	0.0027	0.0226	8.41E-5			
		0.726	0.676	0.753	0.683	0.799	0.716	0.00129	0.0107	0.249	0.0226	8.41E-5					
Energy (MeV)		$^{182}\text{W}(n, p)^{182}\text{Ta}$ reaction cross section (mb)															
		Measured				TALYS - 1.8								EMPIRE - 3.2.2			
8.96± 0.77	0.043±0.003	Ldmodel-1	Ldmodel-2	Ldmodel-3	Ldmodel-4	Ldmodel-5	Ldmodel-6	Levden-0	Levden-1	Levden-2	Levden-3	Levden-4	0.00194				
12.47±0.825	0.793±0.06	0.04813	0.04141	0.12659	0.06359	0.05509	0.05307	0.00964	0.00544	31.0747	0.00964	0.00194	0.00803				
16.63±0.95	4.092±0.28	1.789	1.52	2.33301	1.87	1.86	1.92	0.0842	0.0495	118	0.0842	0.00803	0.163	0.0107			
		10.2	8.89	8.4404	10.2	10.4	10.5	0.163	0.147	124	0.163	0.0107					
Energy (MeV)		$^{154}\text{Gd}(n, 2n)^{153}\text{Gd}$ Cross Section (mb)															
		Measured				TALYS - 1.8								EMPIRE - 3.2.2			
12.47±0.825	1265 ±98	Ldmodel-1	Ldmodel-2	Ldmodel-3	Ldmodel-4	Ldmodel-5	Ldmodel-6	Levden-0	Levden-1	Levden-2	Levden-3	Levden-4	1397				
16.63±0.95	1973±153	1534	1556	1248	1659	1520	1298	1444	1412	22.2	1479	1397	1774	1744			
		1683	1725	1571	1737	1735	1703	1748	1744	65.3	1774	1744					
Energy (MeV)		$^{160}\text{Gd}(n, 2n)^{159}\text{Gd}$ Cross Section (mb)															
		Measured				TALYS - 1.8								EMPIRE - 3.2.2			
12.47±0.825	1913±143	Ldmodel-1	Ldmodel-2	Ldmodel-3	Ldmodel-4	Ldmodel-5	Ldmodel-6	Levden-0	Levden-1	Levden-2	Levden-3	Levden-4	1660				
16.63±0.95	435±33	1938	1919	1765	1935	1901	1828	1669	1679	52.9	1642	1660	999				
		1009	1155	1183	1005	1364	1465	1213	1027	106	1282	999					